MARSTAL DISTRICT HEATING MONITORING DATA EVALUATION FOR THE YEARS 2015-2017

Steinbeis Research Institute
for Solar and Sustainable
Thermal Energy Systems
www.solites.de

solites

ON BEHALF OF

PlanEnergi
Jyllandsgade 1
9520 Skørping
Denmark

Dipl. Ing. Thomas Schmidt

Solites
Steinbeis Research Institute for
Solar and Sustainable Thermal Energy Systems
Meitnerstr. 8, 70563 Stuttgart, Germany
Tel.: +49 711/6732000-0, Fax: +49 711/6732000-99
info@solites.de
www.solites.de

Stuttgart, 28.05.2019

Cover photo: source Marstal Fjernvarme

This work is supportet by
EUDP (project no. 64014-0121)

MARSTAL MONITORING DATA EVALUATION 2015-2017

TABLE OF CONTENTS

---

1. INTRODUCTION

This report documents the evaluation of the monitoring data for the Marstal solar district heating plant for the years 2015 - 2017. This work was done within the Danish EUDP project “Follow up on large scale heat storages in Denmark” (project no. 64014-0121).

The report starts with a summary of the monitoring concept followed by an overview of the overall system heat balances and evaluations that focus on the parts of the solar thermal system: solar collector fields, thermal energy storage and heat pump.

The development of the solar district heating system in Marstal started in 1994, when a 75 m² solar collector test field was installed. After promising results additional 8000 m² of solar collectors were installed shortly afterwards together with a 2 100 m³ buffer tank storage with the purpose to completely cover the summer load of the DH network. In 1999 another 1000 m² solar collectors were added before in 2003 and 2004 another 9 300 m² of solar collectors were added together with a 10 000 m³ seasonal pit thermal energy storage within the European project SUNSTORE 2. In a next step, a 100 % renewable energy supply system was realised within a second European project SUNSTORE 4 in 2012 with the measures listed below. Fig. 1 shows the actual plant concept in Marstal.

Summary of main system components:

Projects SUNSTORE 1 + SUNSTORE 2:

18 300 m²	solar collectors
2 100 m³	buffer storage
10 000 m³	pit thermal energy storage (S2 PTES) – out of operation
400 kW_{th}	heat pump – out of operation
18.3 MW_{th}	bio-oil boilers

Extension and reconstruction of the plant within the EU project SUNSTORE 4 in 2012:

15 000 m²	solar collectors
75 000 m³	pit thermal energy storage (S4 PTES)
4 MW_{th}	biomass boiler
750 kW_{el}	ORC unit (Organic Rankine Cycle)
1.5 MW_{th}	CO_2 heat pump

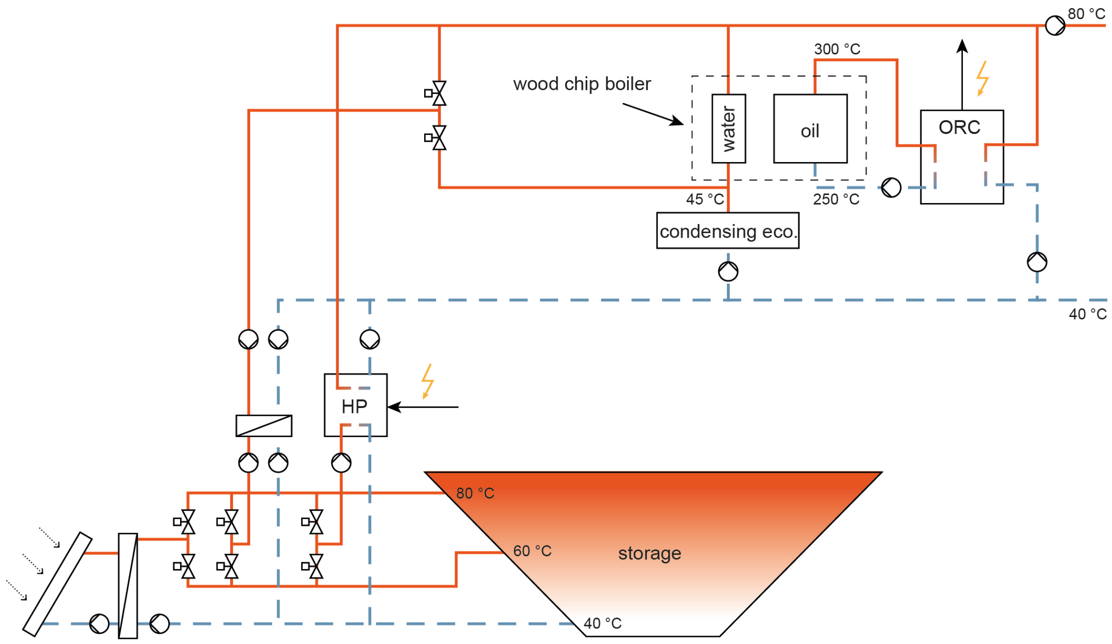

Fig. 1: Marstal SDH system concept

2. MONITORING CONCEPT

This section gives a summary of the monitoring concept for the Marstal Fjernvarme energy system. The monitoring system is described in detail in [Schmidt, 2013].

2.1. Monitoring sensors

Fig. 2 shows the system energy balance and all participating energy flows. The given numbers for heat meters (Q) and electricity meters (E) refer to the PI-diagram for Marstal Fjernvarme - Sunstore 4.

Besides the measurement equipment in the central heating plant, additional monitoring sensors are installed for the evaluation of the pit thermal energy storage (PTES):

- temperature sensors in 3 in-/outlet pipes
- volume flow sensors in 3 in-/outlet pipes
- temperature sensors inside the storage (see Fig. 3)
- ground temperature sensors around the storage (see Fig. 3)
- heat flux sensor inside the cover insulation combined with temperature sensors on top and below the insulation layer at the same position (see Fig. 3)
- water level sensor

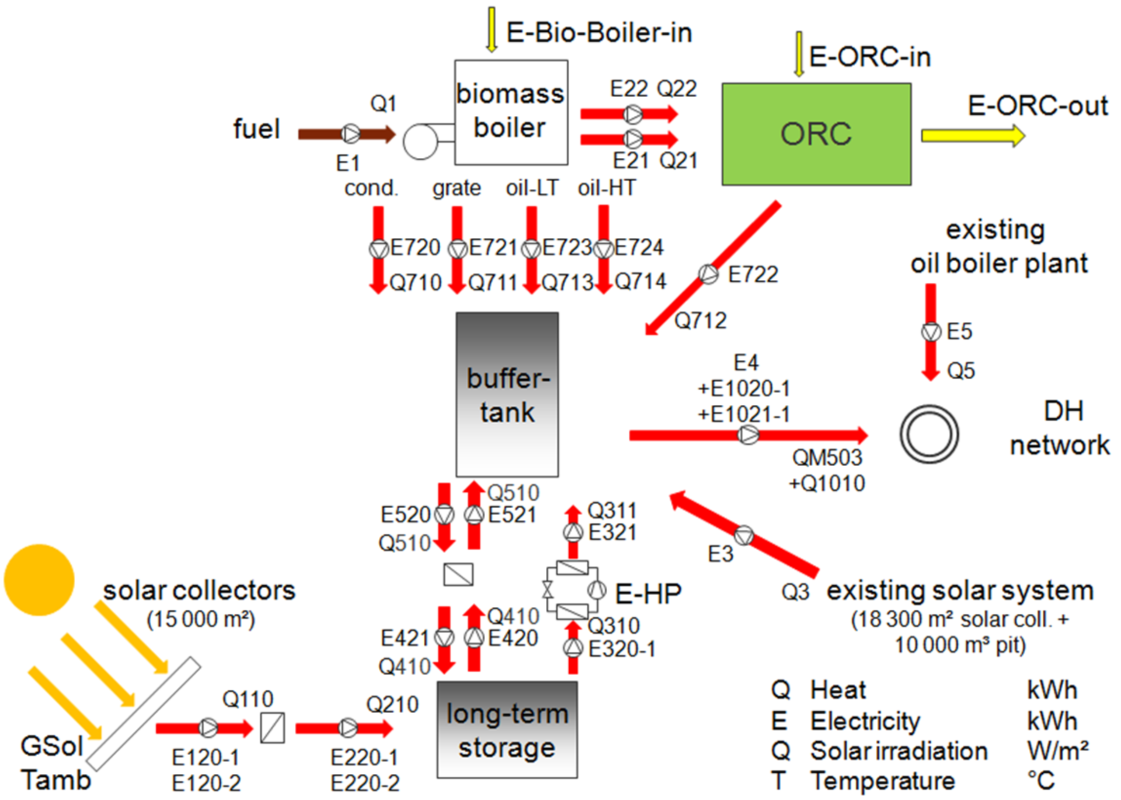

Fig. 2: Overall monitoring concept for the Marstal SDH plant

Fig. 3 shows sensor positions in- and outside the storage volume. There are two vertical temperature sensor strings inside the storage volume – one in the centre of the storage (A1) and one in the middle of the sloped side area (A2). Five temperature sensor strings are placed in the ground around the pit storage. Strings B to D give a detailed view of the temperature development around the storage volume in the south-western quadrant of the storage, strings F and G are equipped with a reduced number of temperature sensors to observe any asymmetrical effects caused e.g. by water movement outside the pit storage.

All monitoring sensors are connected to the SCADA[1] system of the plant, all data is stored in a database in 5-minute time steps.

[1] SCADA: Supervisory Control and Data Acquisition

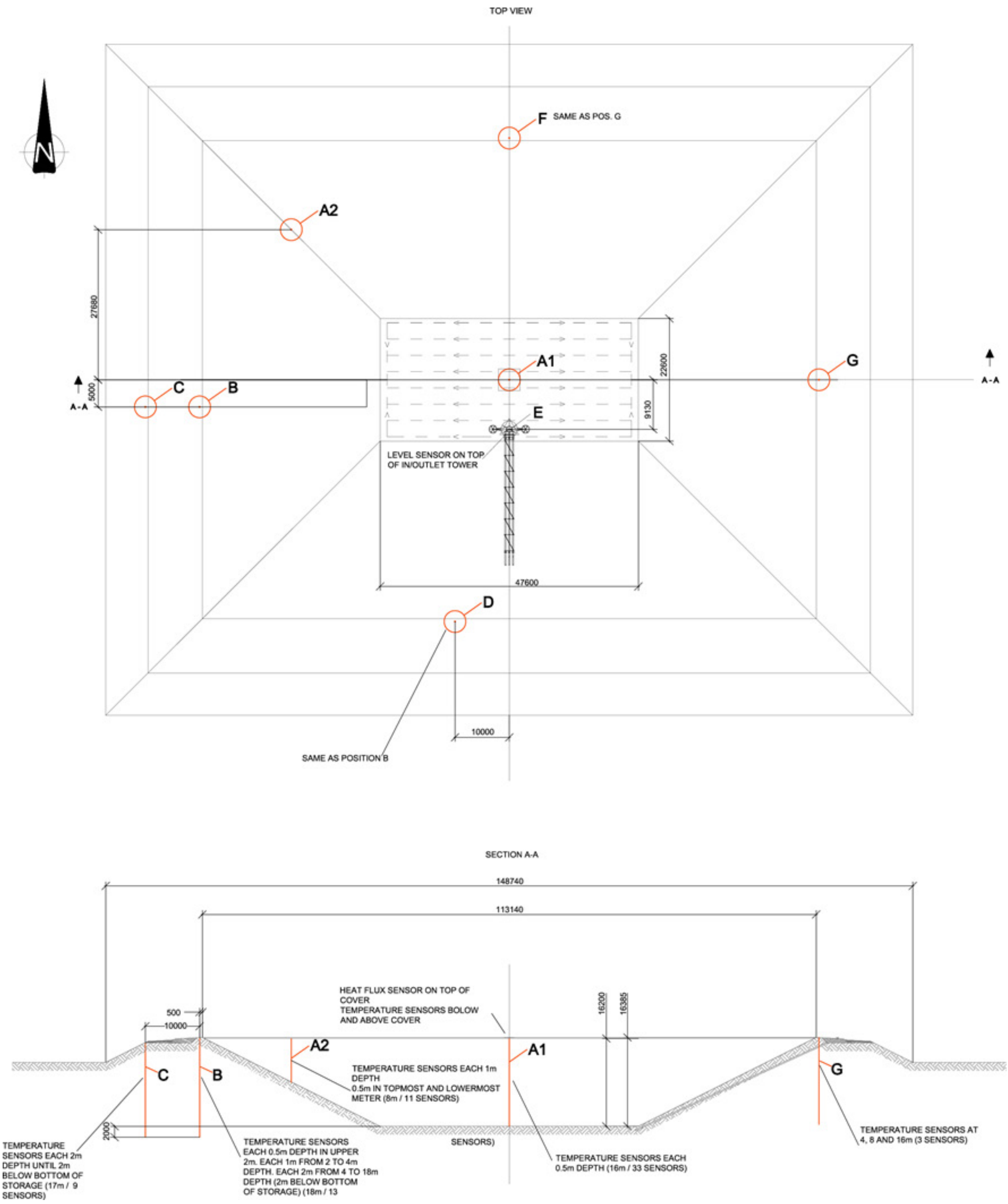

Fig. 3: Monitoring sensors in and around the 75 000 m³ seasonal pit thermal energy storage

2.2. Evaluation

For the comparison of the efficiencies of different system concepts a number of characteristic numbers, often called key performance indicators (KPI) can be calculated. The ones used in the following sections are:

Solar fraction: $$F_{Sol} = \frac{Q_{Load} - Q_{Aux}}{Q_{Load}} = \left(1 - \frac{Q_{Aux}}{Q_{Load}}\right)$$

Q_{Load}: heat supply to the DH network

Q_{Aux}: auxiliary heat delivered to the system (by boilers, CHP, el. demand heat pump etc.)

Solar collector field efficiency $$\eta_{Coll} = \frac{Q_{Coll}}{G_{sol}}$$

Q_{Coll}: heat delivered by the solar collector field

G_{Sol}: global irradiation in solar collector pane

Storage efficiency $$\eta_{STES} = \frac{Q_{STES,out} + dQ_{STES}}{Q_{STES,in}}$$

$Q_{STES,in}$: heat charged into the seasonal thermal energy storage (STES)

$Q_{STES,out}$: heat discharged from the STES

dQ_{STES}: difference in STES internal energy in the period

No. of storage cycles $$N_{cyc} = \frac{Q_{STES,out}}{Q_{STES,max}}$$

$Q_{STES,max}$: maximum heat capacity of the STES

3. SYSTEM HEAT BALANCE

Table 1 gives the main heat balance values as well as a number of performance indicators characterising the SDH system and main components. Fig. 4 shows the yearly heat balance of the entire system.
In 2015 about 29 GWh of heat were delivered to the district heating (DH) network. The calculated solar fraction in that year is 39 %. 59 % of the heat was produced by a biomass boiler that is mostly supplying an ORC unit and sometimes delivering heat directly to the DH network. The electricity demand of the heat pump accounted for 2 % of the total heat delivery.
Energy flow diagrams of the yearly system heat balances in 2015, 2016 and 2017 are presented in Fig. 4 to Fig. 6. Fig. 50 in Annex 1 shows the corresponding design figures. The design solar fraction value is 32 %.

Deviations in heat balances are due to rounding, measurement errors or not measured energy flow streams (e.g. thermal losses of storages).

Table 1: Overview of evaluation results for the considered evaluation period in Marstal

		2015	2016	2017
solar irradation on solar collectors	*MWh*	40381	36978	34533
heat from solar collectors	*MWh*	12990	11848	11759
solar heat direct to system	*MWh*	5177	4743	4992
heat charged into PTES	*MWh*	7813	7104	6768
heat discharged from PTES	*MWh*	5758	5322	3471
PTES internal energy change*)	*MWh*	-569	-642	-858
PTES thermal losses	*MWh*	2624	2424	4155
heat pump heat delivery	*MWh*	2199	3468	3595
heat pump electricity demand	*MWh*	671	1045	1117
heat from biomass boiler and ORC	*MWh*	16500	15445	17169
ORC electricity production	*MWh*	2854	2543	1243
heat from oilboiler plant	*MWh*	35	2193	3823
heat delivery to DH	*MWh*	29043	30143	30868
key performance indicators				
solar collector field efficiency	*%*	32	32	34
PTES storage efficiency	*%*	66	66	39
PTES no. of storage cycles	-	1.1	1.0	0.7
PTES maximum temperature	*°C*	84	82	69
PTES minimum temperature	*°C*	20	20	13
PTES used heat capacity	*MWh*	5430	5320	4830
heat pump COP	-	3.3	3.3	3.2
solar fraction	*%*	39	35	28
biomass fraction	*%*	59	54	56
oil boiler fraction	*%*	0	8	13
heat pump electricity fraction	*%*	2	4	4

*): negative value for energy decrease

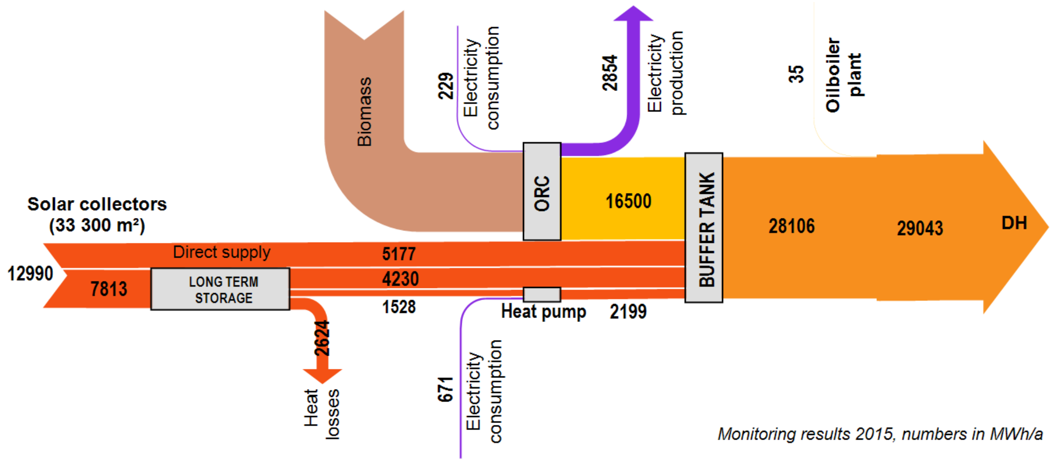

Fig. 4: Heat flow diagram according to monitoring data for 2015

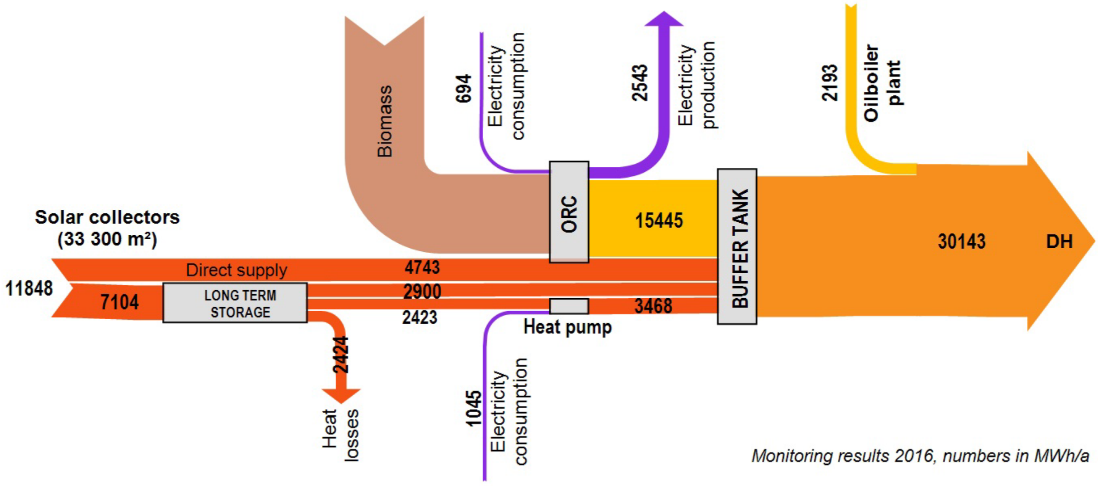

Fig. 5: Heat flow diagram according to monitoring data for 2016

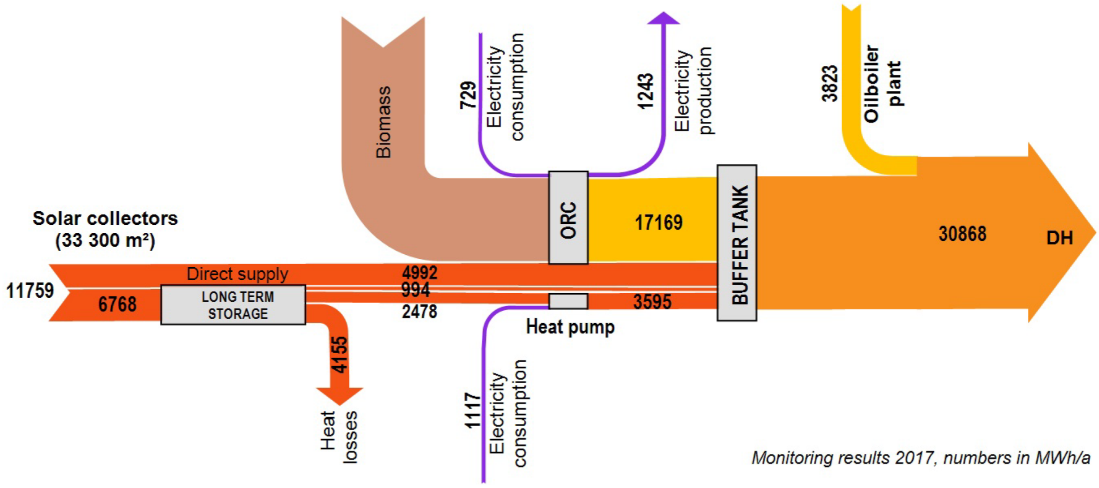

Fig. 6: Heat flow diagram according to monitoring data for 2017

In Fig. 7 to Fig. 9 the monthly heat balances of the overall system for the years 2015 to 2017 are illustrated. The narrow bars in the front show the heat consumption as well as the charging of the PTES, the wide bars in the background represent the different heat producers as well as the discharging of the PTES.

Fig. 10 to Fig. 12 show the heat load and temperature development in the DH network to Marstal for the years 2015 to 2017. The network temperatures are fairly stable in the entire evaluation period with supply temperatures between 70 and 75 °C and return temperatures of around 35 °C in the winter period and 40 to 45 °C during summer.

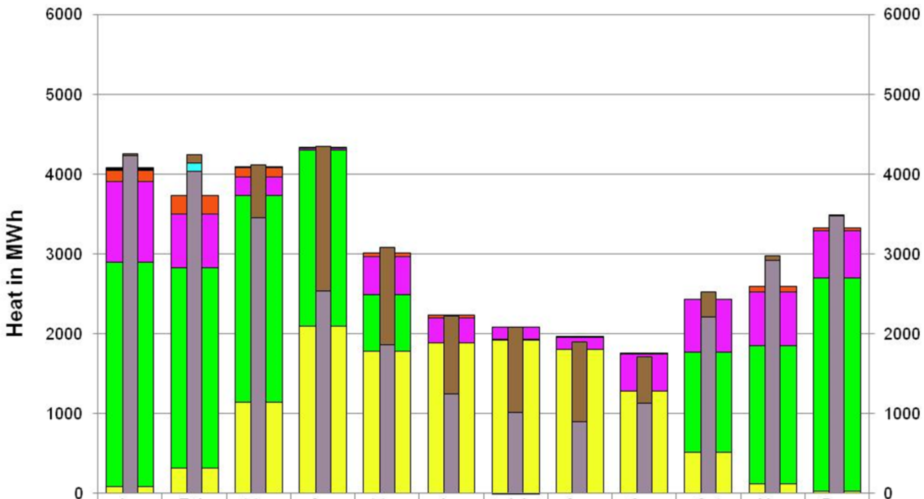

	Jan 2015	Feb 2015	Mar 2015	Apr 2015	May 2015	Jun 2015	Jul 2015	Aug 2015	Sep 2015	Oct 2015	Nov 2015	Dec 2015
Oil Boilers	32	0	3	0	0	0	0	0	0	0	0	0
Electricity consumption Heat Pump	140	232	113	7	41	33	0	0	0	0	70	36
Discharging S4 PTES	1018	672	230	20	485	314	159	140	469	660	678	589
Biomass Boiler + ORC	2804	2513	2595	2210	703	0	9	0	0	1251	1737	2678
Solar Collectors	89	317	1144	2098	1784	1886	1919	1811	1282	518	116	26
Charging S4 PTES	22	111	659	1813	1214	974	1074	995	584	312	52	2
Sunmark cooling	0	103	0	0	0	0	0	0	0	0	7	0
Total heat supply	4239	4035	3456	2535	1868	1253	1013	900	1134	2215	2919	3475

Fig. 7: Monthly system heat balance for 2015

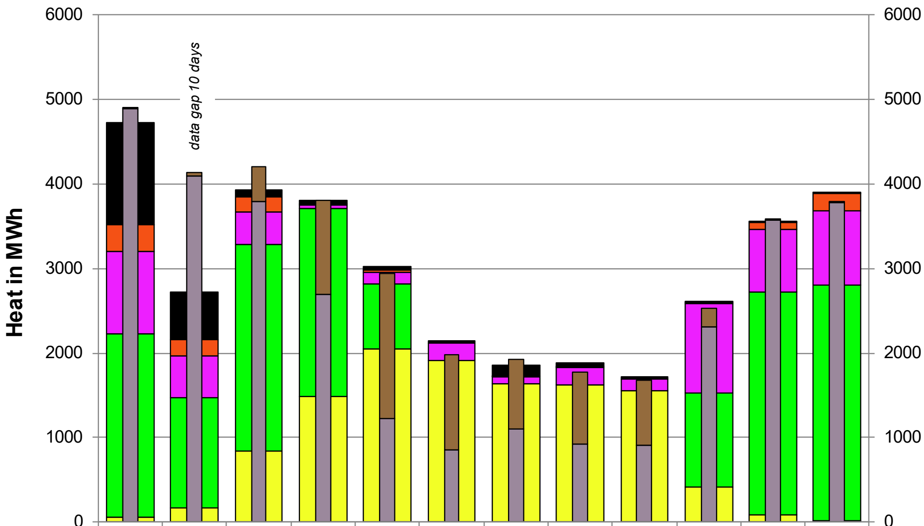

	Jan 2016	Feb 2016	Mar 2016	Apr 2016	May 2016	Jun 2016	Jul 2016	Aug 2016	Sep 2016	Oct 2016	Nov 2016	Dec 2016
Oil Boilers	1209	556	82	32	44	25	132	62	22	6	22	1
Electricity consumption Heat Pump	317	192	178	18	30	0	9	1	0	11	80	210
Discharging S4 PTES	970	493	387	41	141	201	75	206	144	1051	739	874
Biomass Boiler + ORC	2167	1307	2439	2228	765	0	0	0	0	1111	2642	2785
Solar Collectors	61	168	839	1484	2049	1916	1639	1622	1550	422	80	17
Charging S4 PTES	11	52	412	1116	1712	1130	819	843	769	219	15	5
Total heat supply	4889	4089	3798	2692	1224	852	1103	927	914	2304	3570	3782

Fig. 8: Monthly system heat balance for 2016

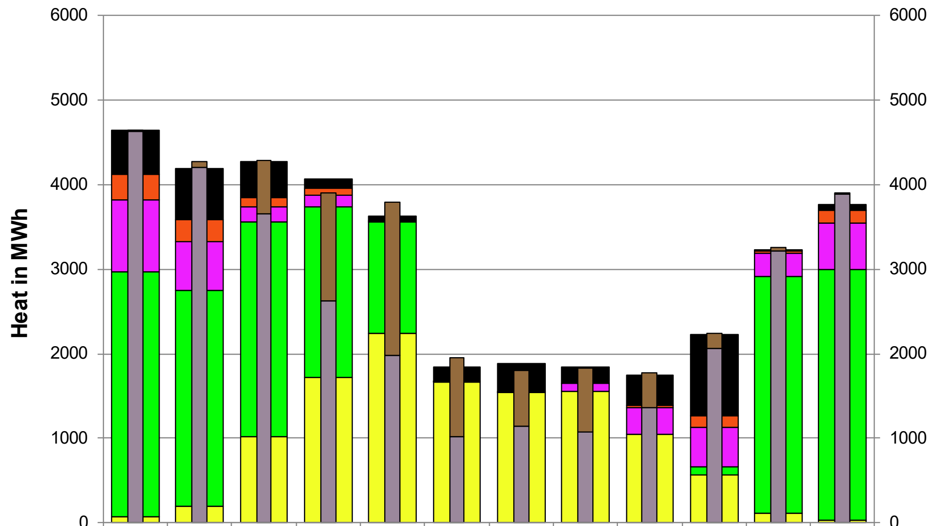

	Jan 2017	Feb 2017	Mar 2017	Apr 2017	May 2017	Jun 2017	Jul 2017	Aug 2017	Sep 2017	Oct 2017	Nov 2017	Dec 2017
Oil Boilers	519	604	435	116	51	179	341	196	345	960	9	69
Electricity consumption Heat Pump	312	262	99	81	0	0	0	0	36	144	23	160
Discharging S4 PTES	843	574	183	137	18	1	4	103	318	465	281	545
Biomass Boiler + ORC	2898	2547	2537	2015	1315	0	0	0	0	94	2795	2968
Solar Collectors	72	201	1022	1723	2242	1660	1541	1549	1041	566	116	25
Charging S4 PTES	13	74	633	1276	1808	933	659	759	401	172	38	0
Total heat supply	4636	4204	3649	2625	1984	1020	1146	1069	1366	2064	3215	3892

Fig. 9: Monthly system heat balance for 2017

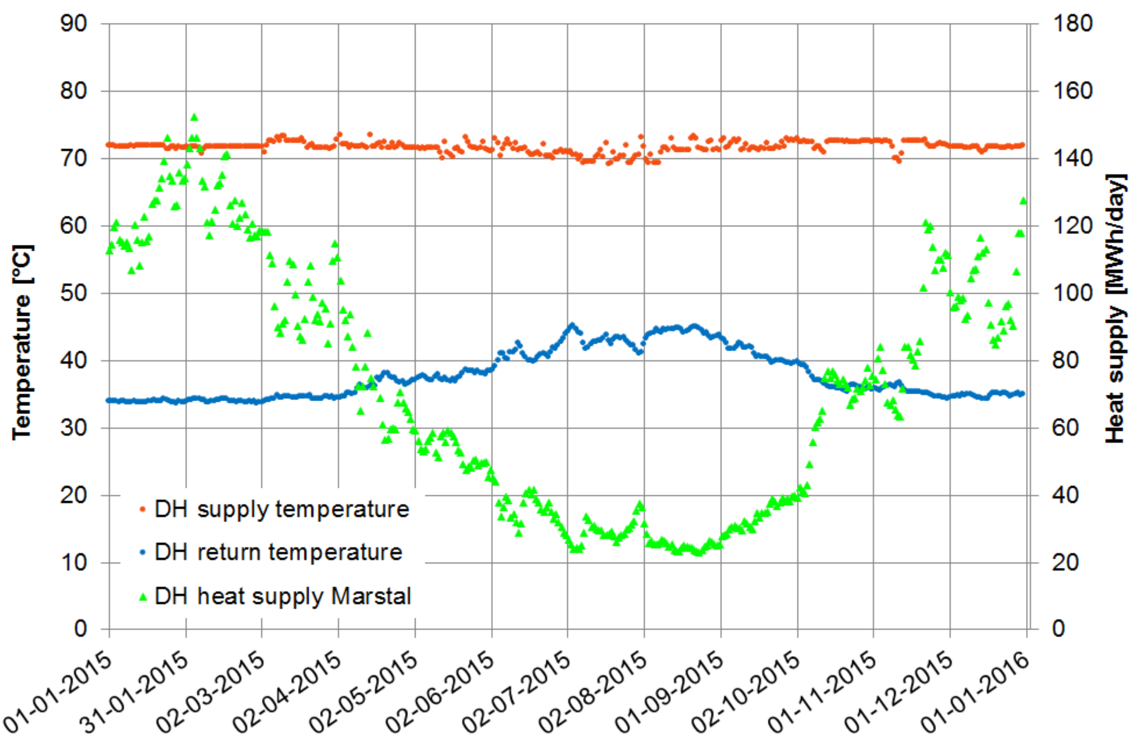

Fig. 10: DH heat supply to Marstal in 2015 (daily values)

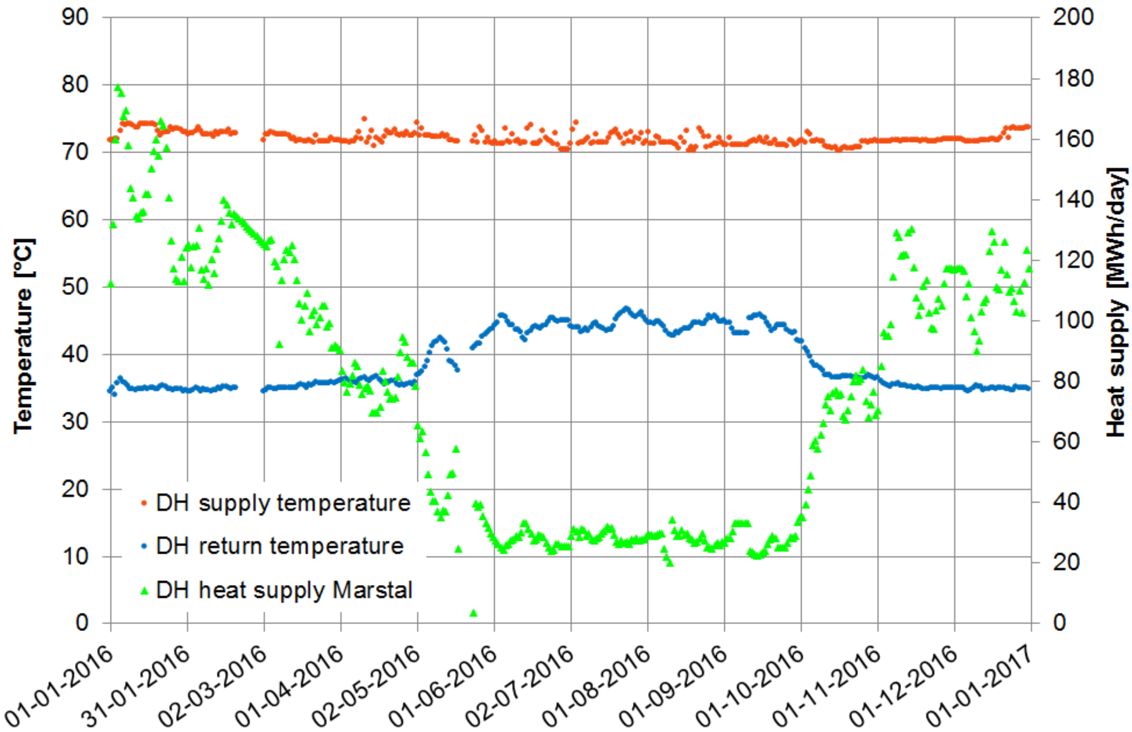

Fig. 11: DH heat supply to Marstal in 2016 (daily values)

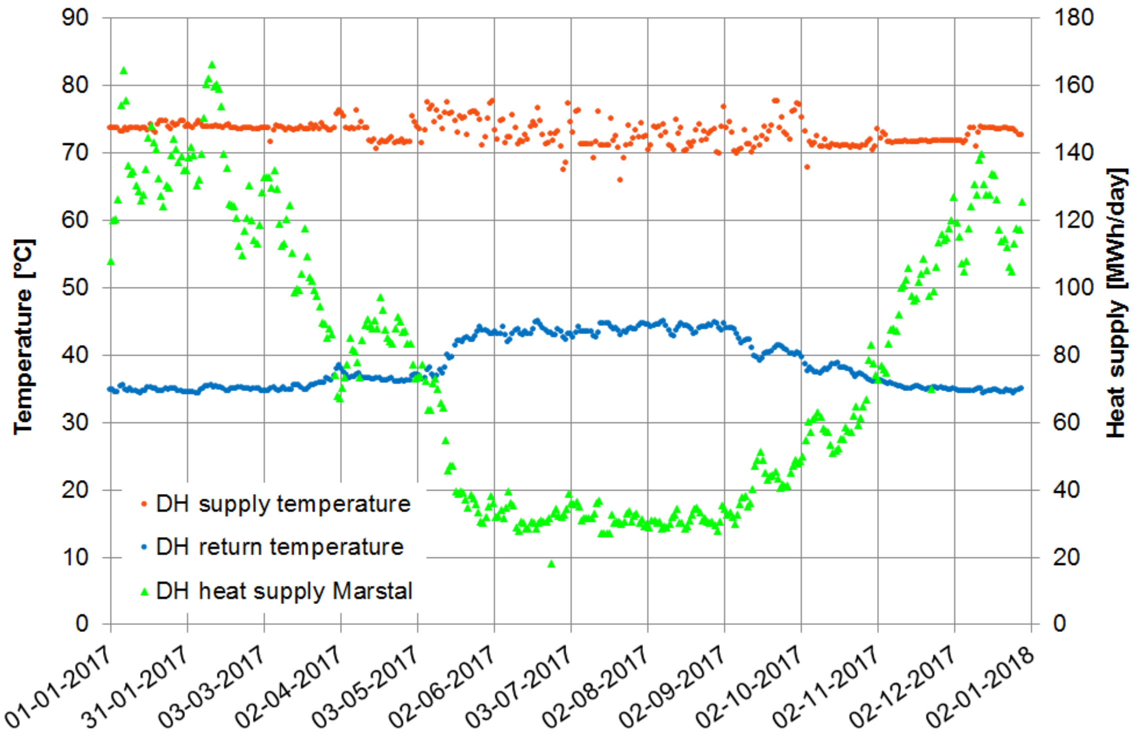

Fig. 12: DH heat supply to Marstal in 2017 (daily values)

4. SOLAR COLLECTORS

Fig. 13 to Fig. 15 present the heat production of the solar collector fields. In total 12990 MWh of solar heat were delivered to the system in 2015, 11848 MWh in 2016 and 11759 MWh in 2017.

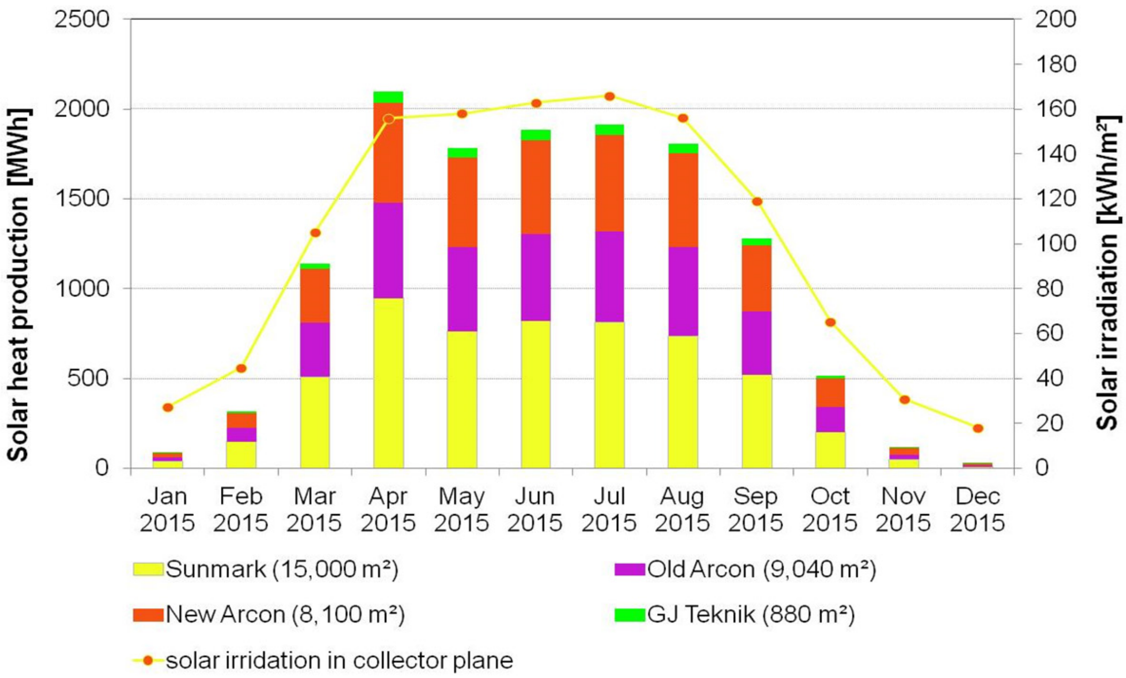

Fig. 13: Solar collector heat production in 2015

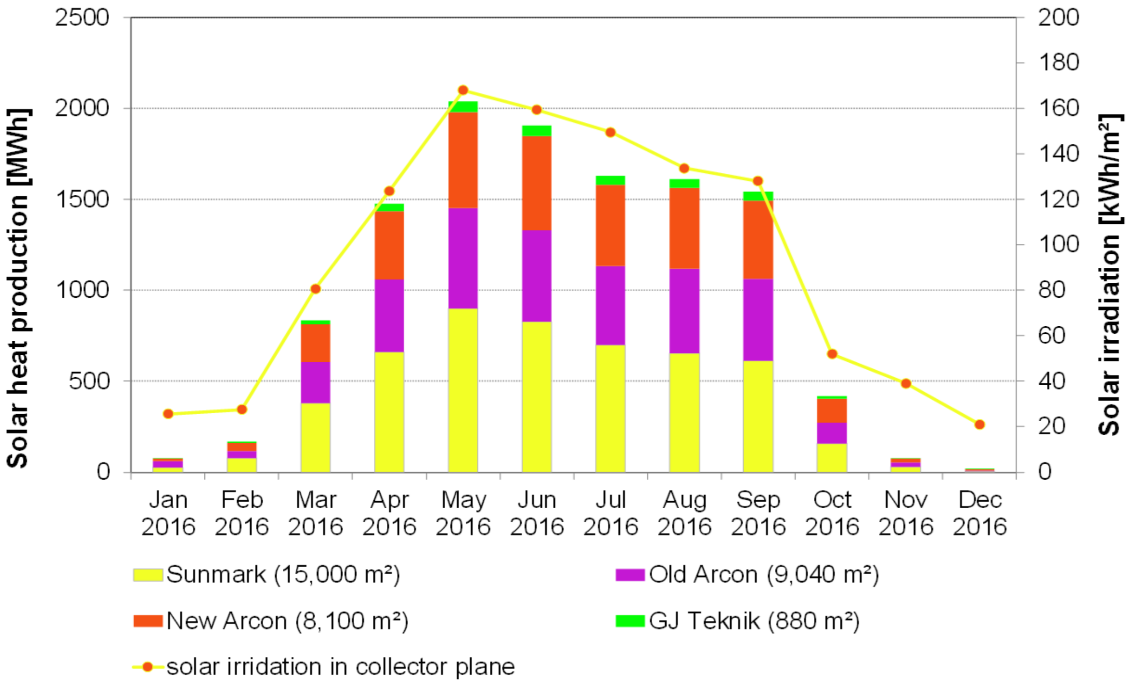

Fig. 14: Solar collector heat production in 2016

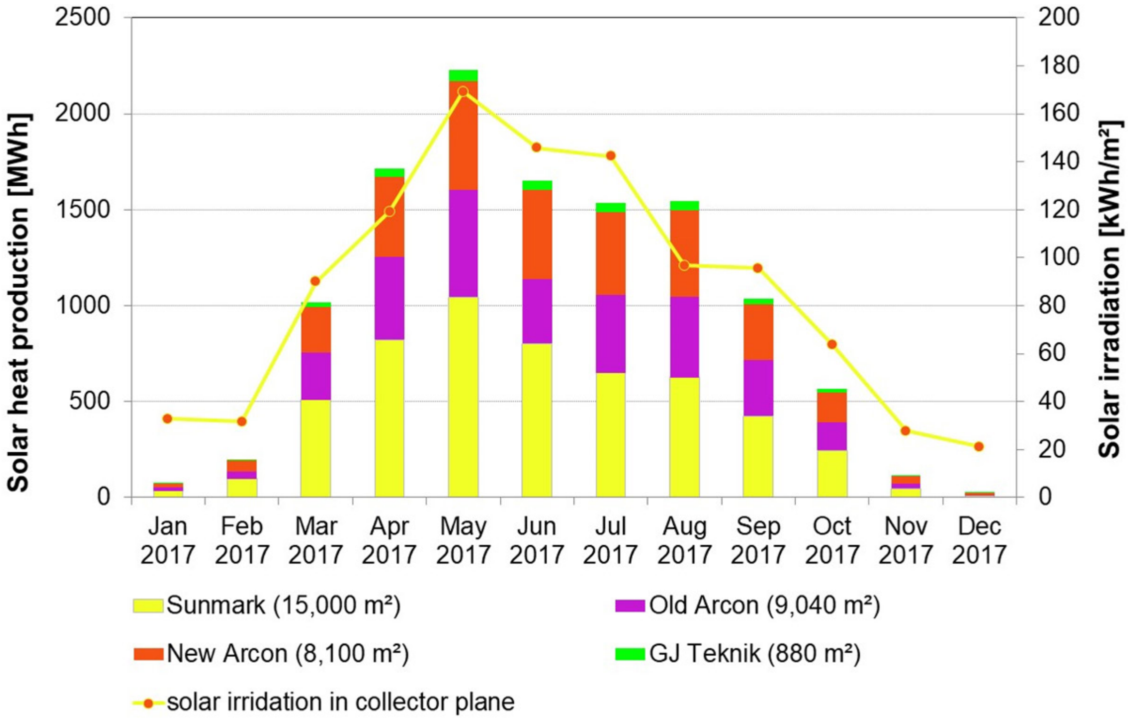

Fig. 15: Solar collector heat production in 2017

Values for solar heat production per m² of solar collector aperture area and year are shown in Fig. 16 to Fig. 18 for the years 2015 to 2017. They range from 323 to 446 kWh/m²a for the different solar collector fields in the three years.

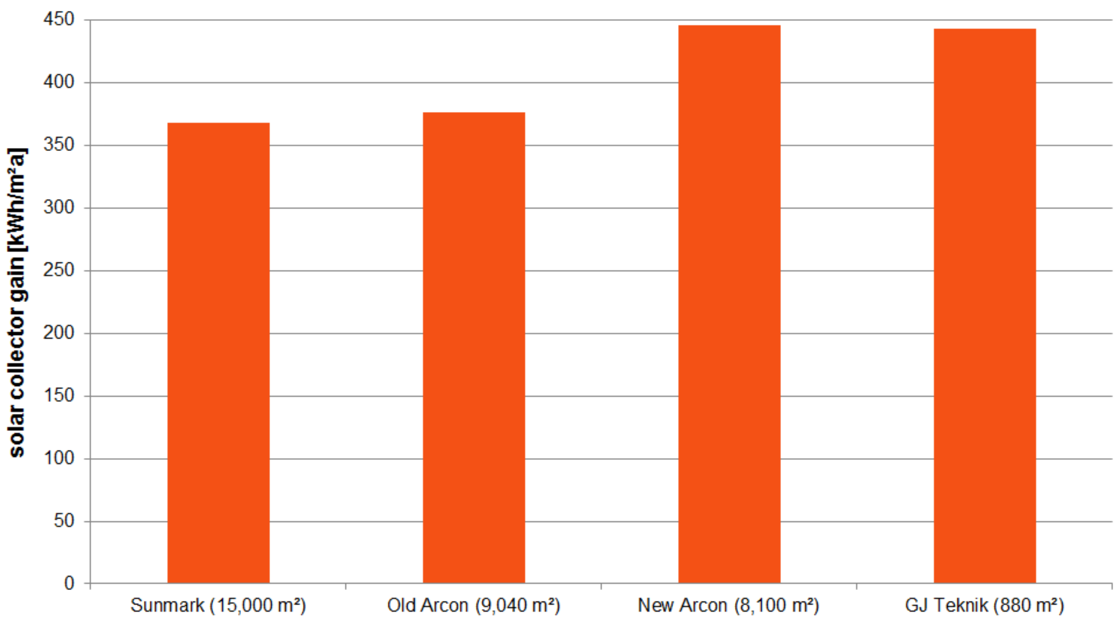

Fig. 16: Solar collector (aperture-) area-related heat production of main solar collector fields in 2015

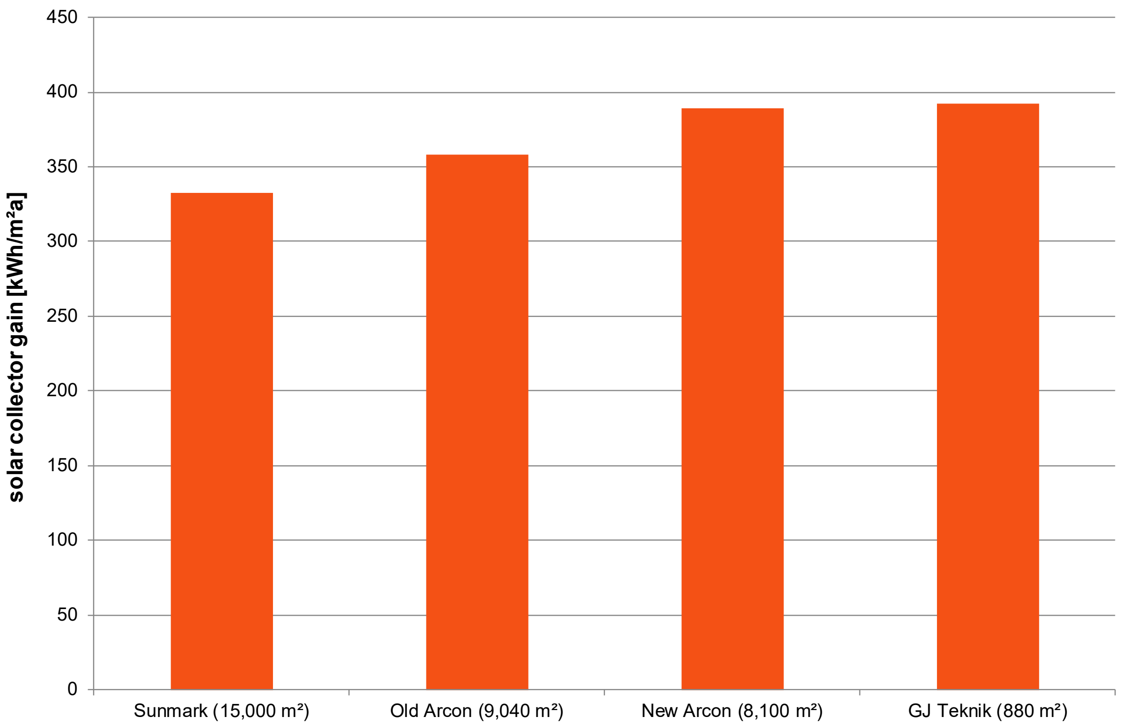

Fig. 17: Solar collector (aperture-) area-related heat production of main solar collector fields in 2016

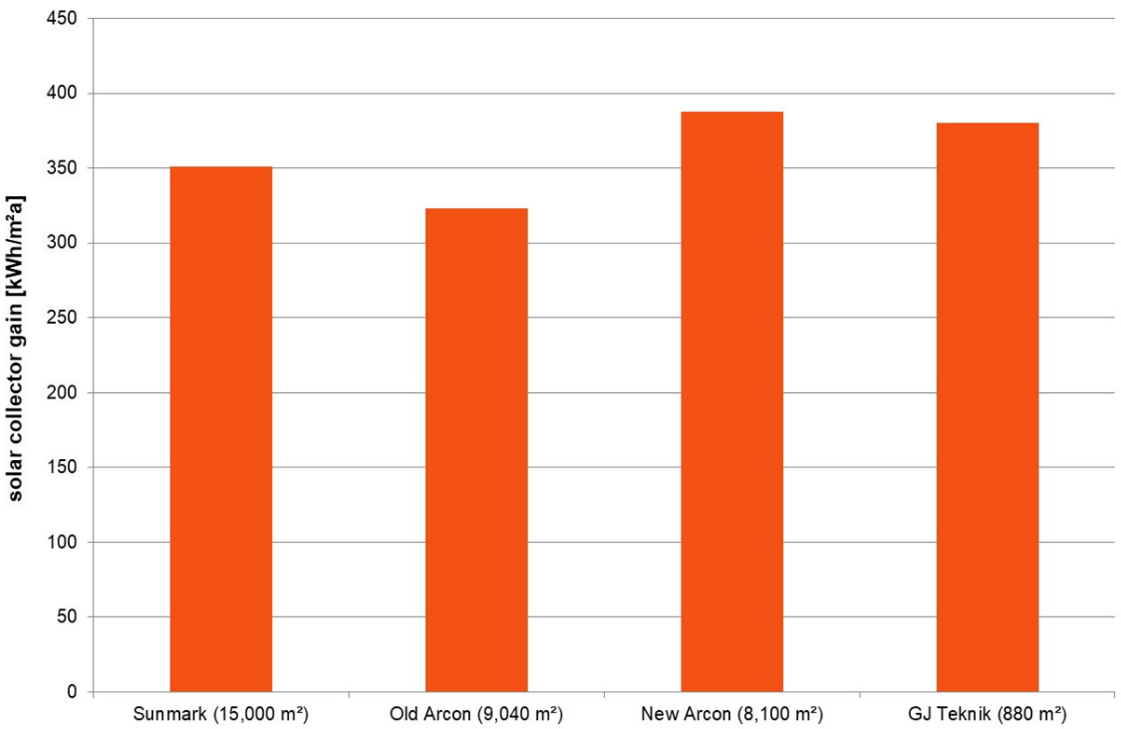

Fig. 18: Solar collector (aperture-) area-related heat production of main solar collector fields in 2017

Differences in the area-related solar heat production values are explainable by differences in solar irradiation in the different years, different solar collector products and differences in operational conditions for the solar collector fields as can be seen in Fig. 19 to Fig. 22. The Sunmark solar collector field is hydraulically connected to the PTES and is operated mainly to charge the storage. The other solar collector fields are hydraulically connected to the central system and most of the time deliver their heat either directly to the district heating network or to the buffer storage. The different operation conditions resulting from this are clearly visible when comparing especially the return temperature values of Fig. 19 with Fig. 20 to Fig. 22.

Fig. 19 shows the operating conditions of the Sunmark solar collector field. Return temperatures are strongly connected to the bottom temperatures of the PTES and vary from approx. 10 °C to 60 °C, see also section 5.1. Supply temperatures increase from spring to end of summer following the return temperatures.

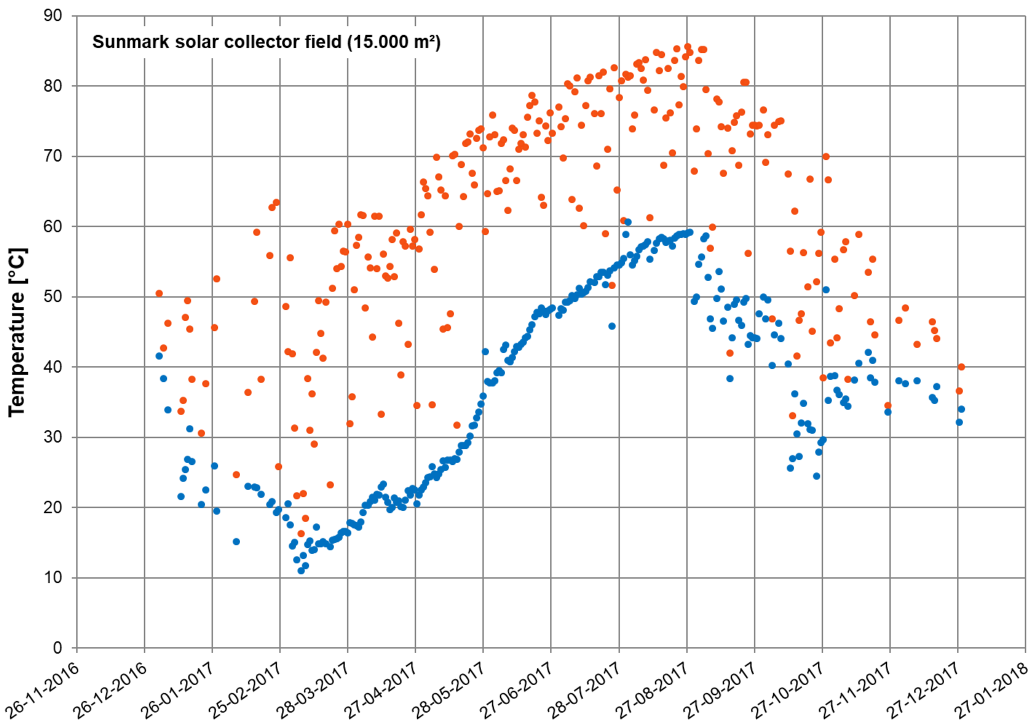

Fig. 19: Operating conditions of the Sunmark solar collector field in 2017 (flow weighted daily mean values measured at the water side of the solar heat exchanger)

In Fig. 20 to Fig. 22 the operating conditions for the solar collector fields connected to the central system can be seen. From March to September solar heat production temperatures are mostly above 75 °C, inlet temperatures to the solar collector circuit are between 30 and 50 °C.

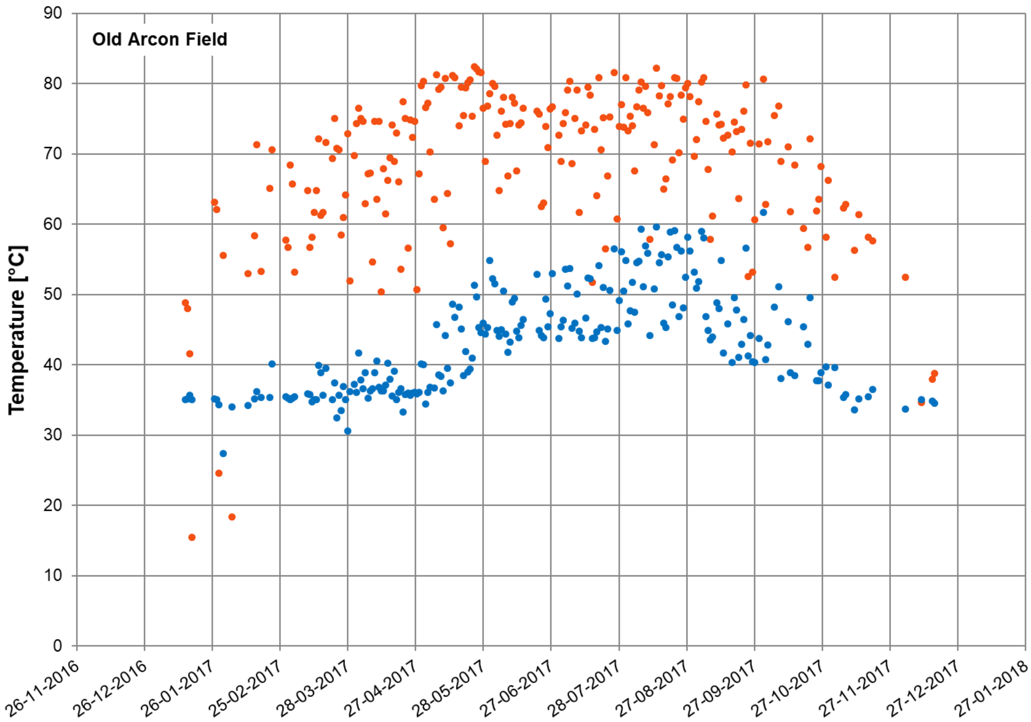

Fig. 20: Operating conditions of the "Old Arcon" solar collector field in 2017 (flow weighted daily mean values measured at the water side of the solar heat exchanger)

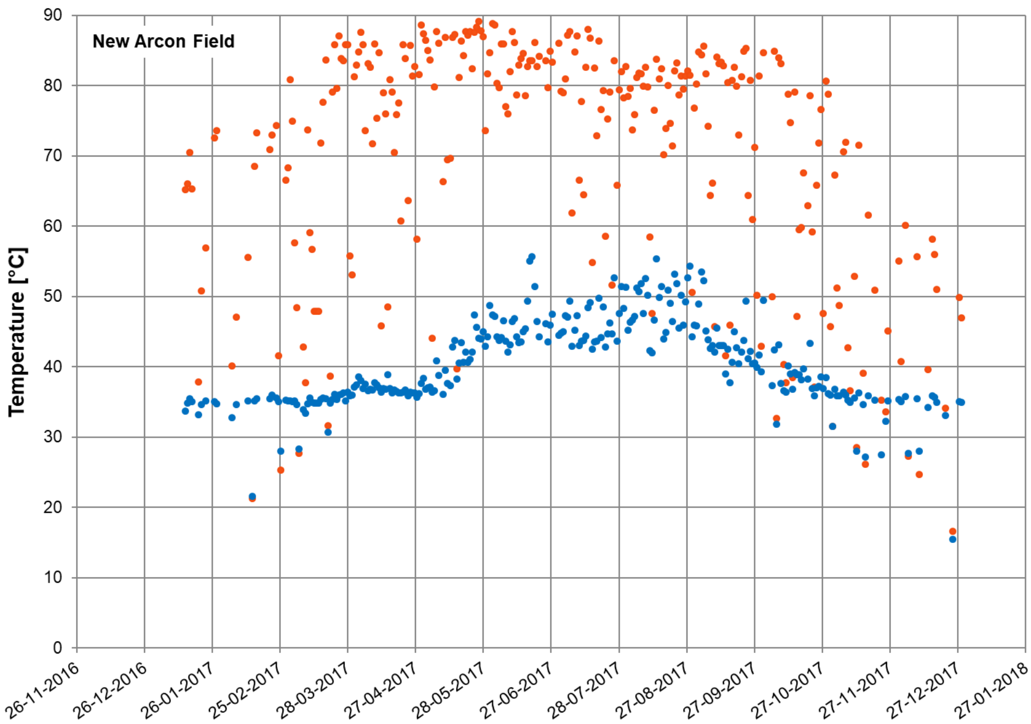

Fig. 21: Operating conditions of the "New Arcon" solar collector fields in 2017 (flow weighted daily mean values measured at the water side of the solar heat exchanger)

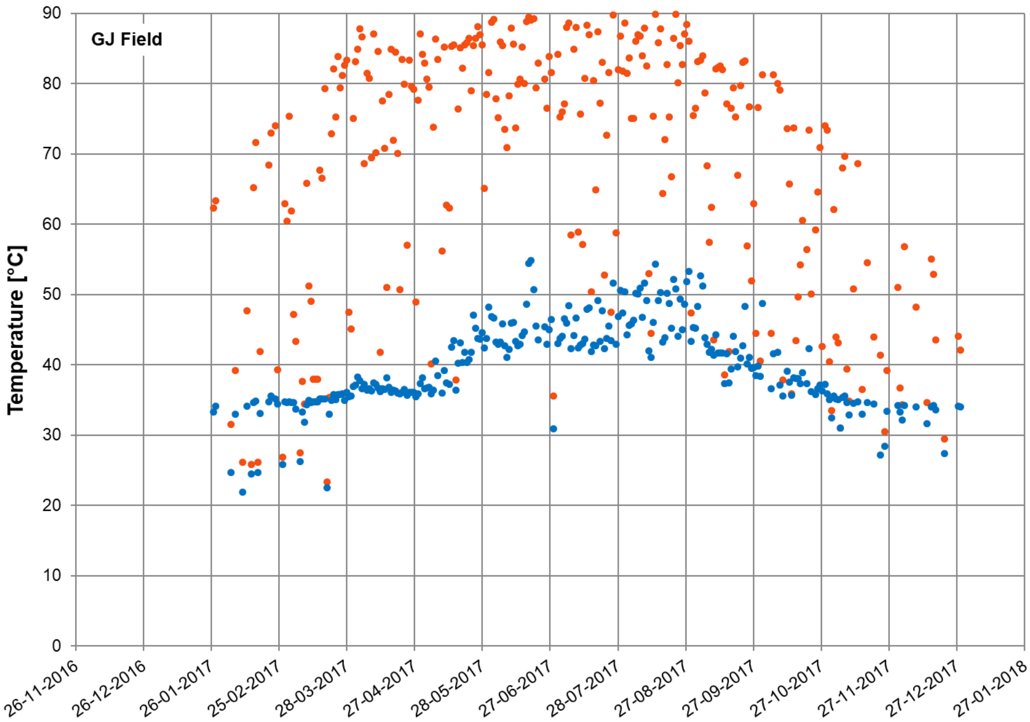

Fig. 22: Operating conditions of the GJ solar collector field in 2017 (flow weighted daily mean values measured at the water side of the solar heat exchanger)

Fig. 23 and Fig. 24 show the daily solar heat productions of the three largest solar collector fields as a function of the daily irradiation into the corresponding solar collector area. The input-output diagrams show a rather uniform solar heat production with only few spikes indicating a robust operation without serious failures.

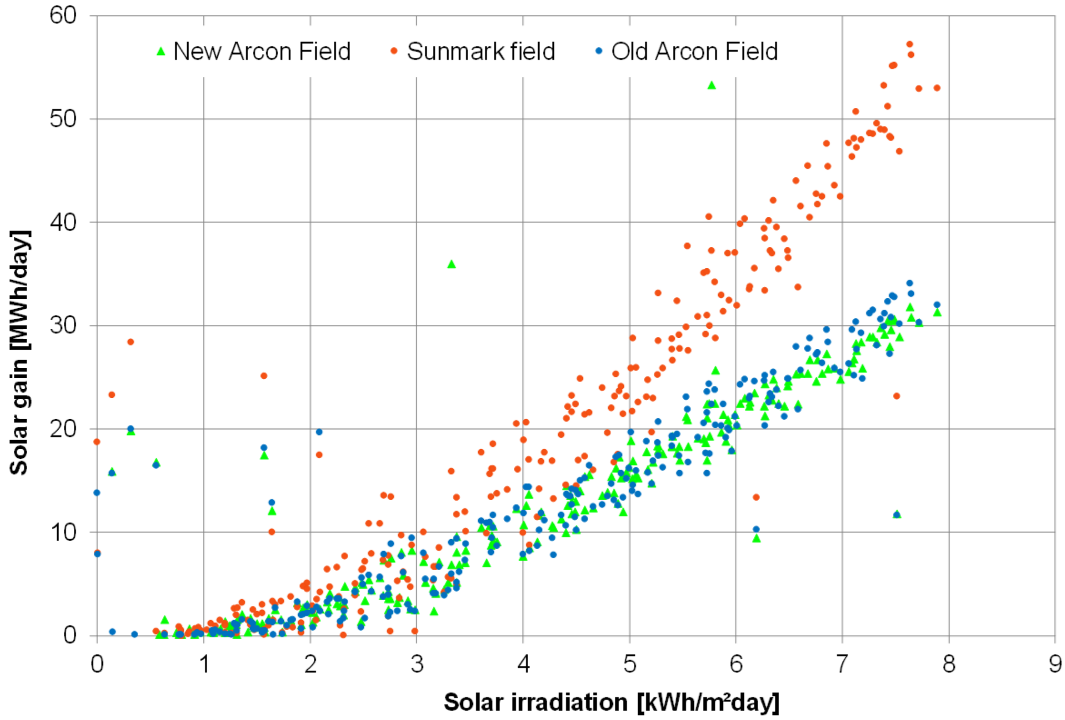

Fig. 23: Heat production of the three largest solar collector fields as a function of the solar irradiation into corresponding solar collector area for 2016

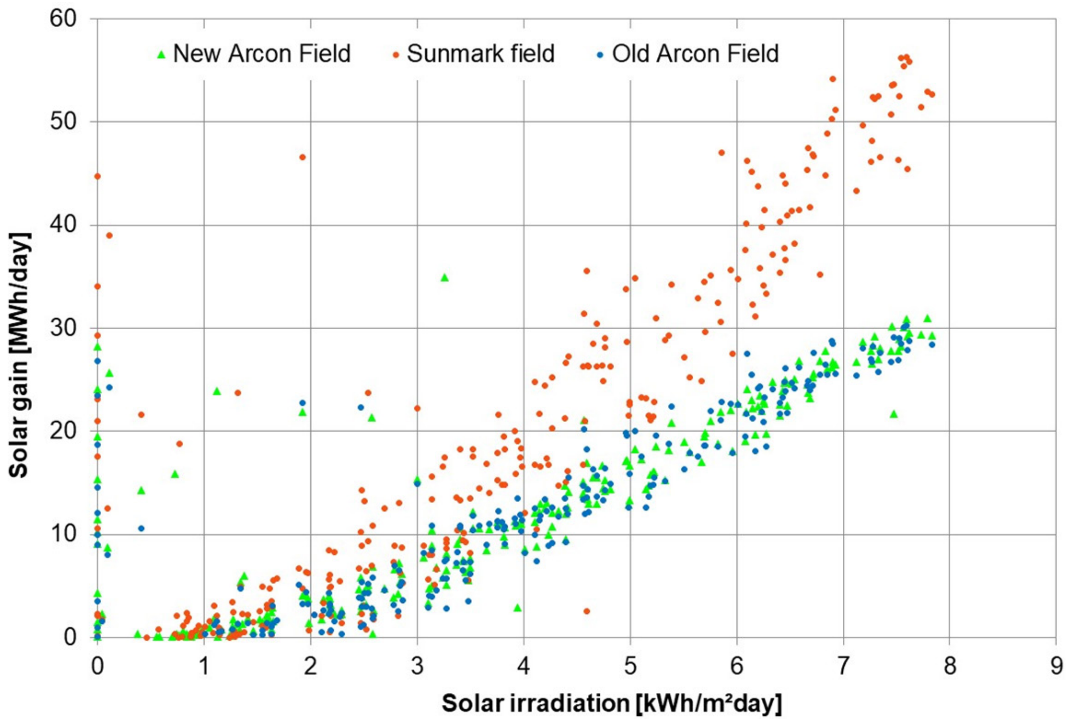

Fig. 24: Heat production of the three largest solar collector fields as a function of the solar irradiation into corresponding solar collector area for 2017

5. PIT THERMAL ENERGY STORAGE

In Fig. 25, the yearly energy balance for the PTES is shown for 2015. 7813 MWh of solar heat were charged into the storage and 5758 MWh were discharged to the system. The internal energy content of the storage is calculated based on temperature sensors that are installed in the water volume every 0.5 m in vertical direction. In 2015, the energy content in the storage at the end of the year was 569 MWh below the one at the beginning of the year. According to the storage heat balance the thermal losses, that were transferred to the surrounding ground and the ambient air, accounted for 2624 MWh. The maximum and minimum temperatures in the storage volume in 2015 were 84 °C and 20 °C respectively.

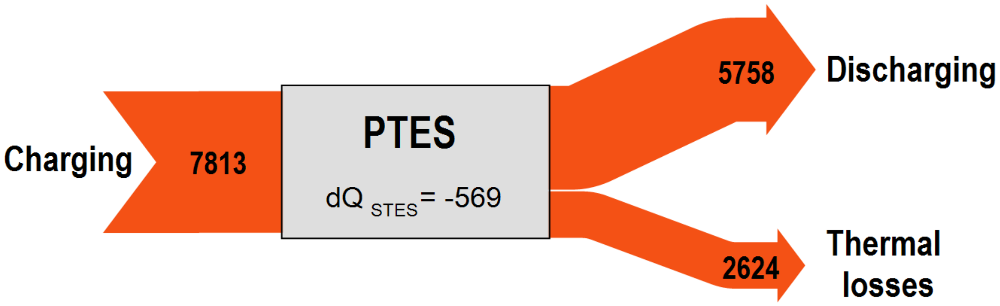

Fig. 25: Yearly PTES heat balance for 2015 (numbers in MWh; dQ_{STES}: internal energy change in the storage, negative value for energy decrease)

The evaluated storage efficiency of 66% for 2015 is a little higher than the design value of 61%. A storage cycle number of 1.1 means that the heat capacity of the storage was used 1.1 times, representing a pure seasonal operation.
Fig. 26 and Fig. 27 show the PTES heat balances for 2016 and 2017. The corresponding values for storage efficiency and cycle number are listed in Table 1.

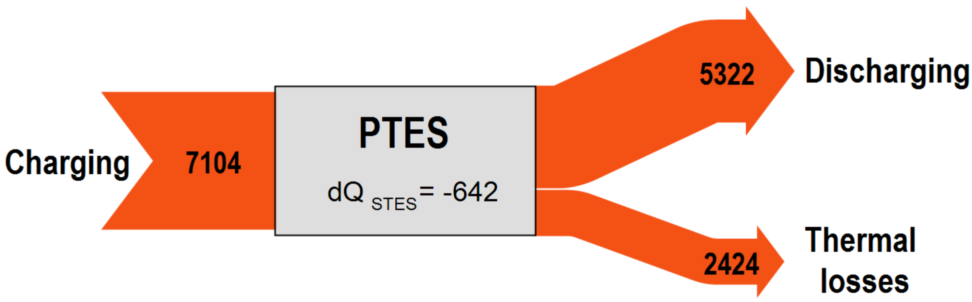

Fig. 26: Yearly PTES heat balance for 2016 (numbers in MWh; dQ_{STES}: internal energy change in the storage, negative value for energy decrease)

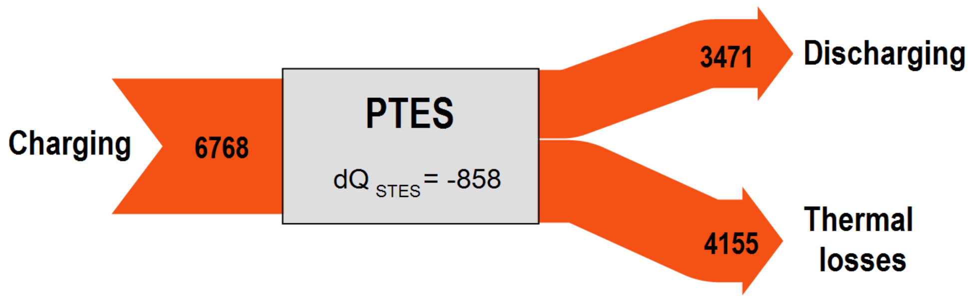

Fig. 27: Yearly PTES heat balance for 2017 (numbers in MWh; dQ_{STES}: internal energy change in the storage, negative value for energy decrease)

In 2017 the thermal losses of the PTES were higher than in the years before. This also led to a lower storage efficiency in this year. The reason is most probably a humidification of the cover insulation by rain water, which has entered the cover construction through a leakage. This is further investigated and will be fixed in the near future.

The seasonal operation of the PTES can be seen in the monthly charged and discharged amounts of heat presented in Fig. 28. The main charging processes are in summer and the main discharging processes in winter.

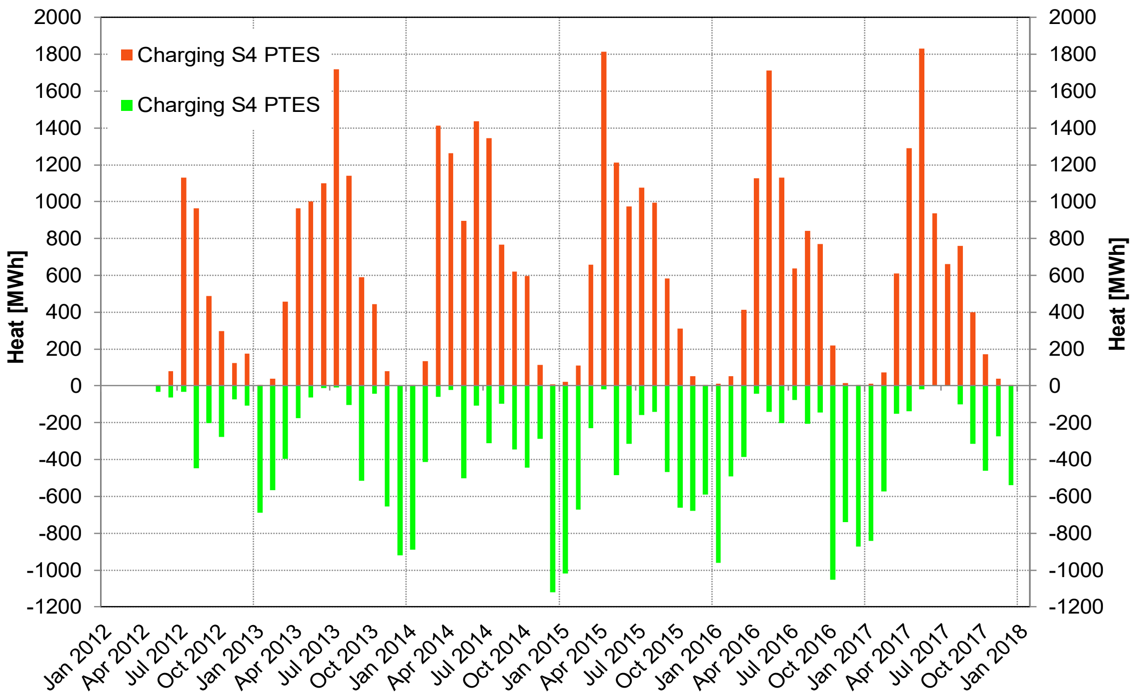

Fig. 28: Monthly heat balance for the PTES since beginning of operation in 2012 until 2017

5.1. PTES temperature development

In Fig. 29, the temperature development in the storage is illustrated from 2013 to 2017. Again, the seasonal operation is clearly visible with a charging period from around March to September and a discharging period from around September to March. Minimum temperatures in March are around 30 °C at the top of the storage and 15 to 20 °C at the bottom. Maximum temperatures in September reach some 85 °C at the top and around 70 °C at the bottom. In 2017, the temperatures in summer were about 10 K lower compared to the two years before. The highest thermal stratification, that means the largest temperature differences between the top and the bottom of the storage, of around 30 K can be seen in spring and autumn.

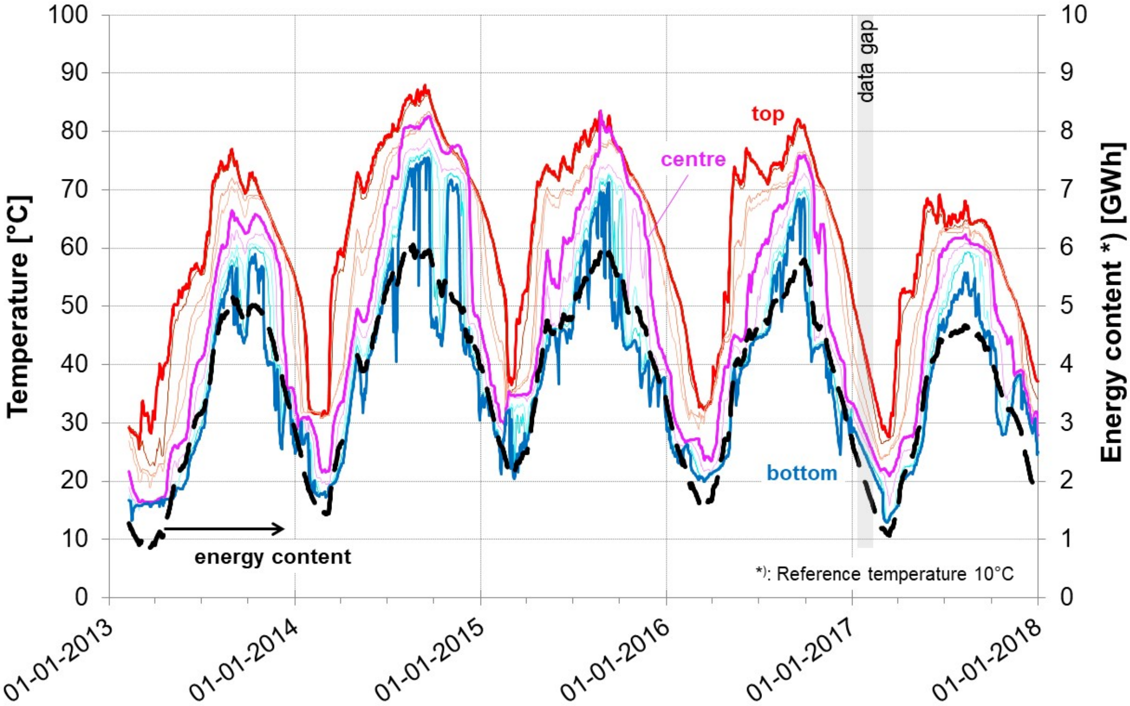

Fig. 29: Temperature and energy content development inside the PTES (daily mean values)

In Fig. 30, the temperature development in the storage is illustrated in a vertical view for 2017 in monthly values. This illustration allows a good presentation of the charging states in the course of the year as well as the thermal stratification from the top of the storage volume to the bottom. In August, the highest charging state can be seen with a thermal stratification of approximately 10 K. The lowest charging state was in March. The highest levels of thermal stratification occurred during the main charging period in April and May.

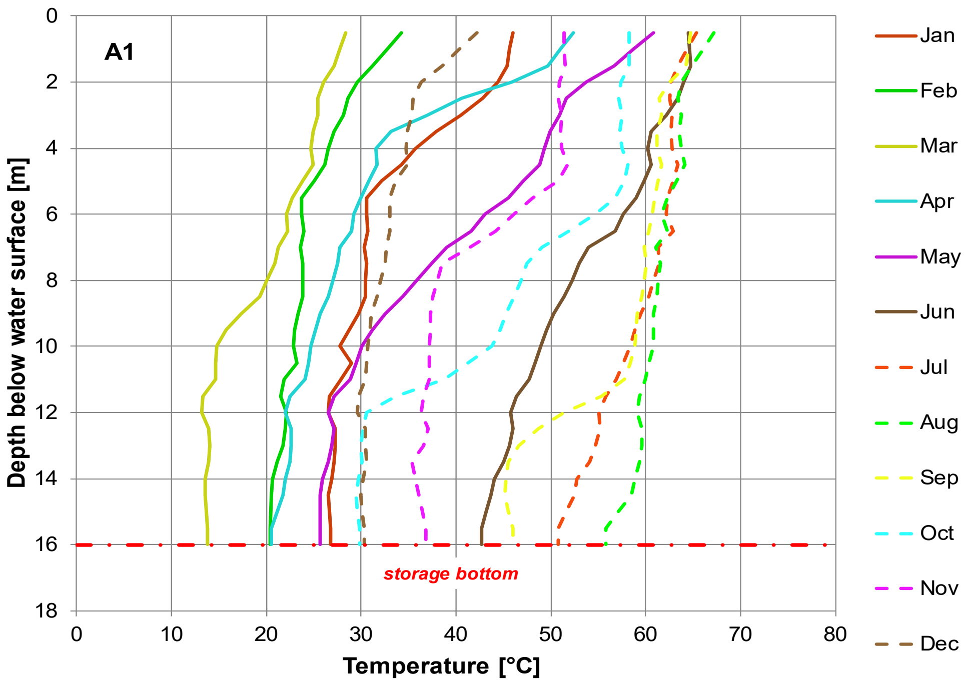

Fig. 30: Monthly PTES temperature development in 2017 (daily mean values at mid of the months)

Fig. 31 to Fig. 33 illustrate the temperatures in the three pipes connecting the PTES to the heating plant in 2015 to 2017. Depending on the operation mode of the storage (e.g. charging or discharging) the flow directions in all of the three pipes can be either into or out of the storage.

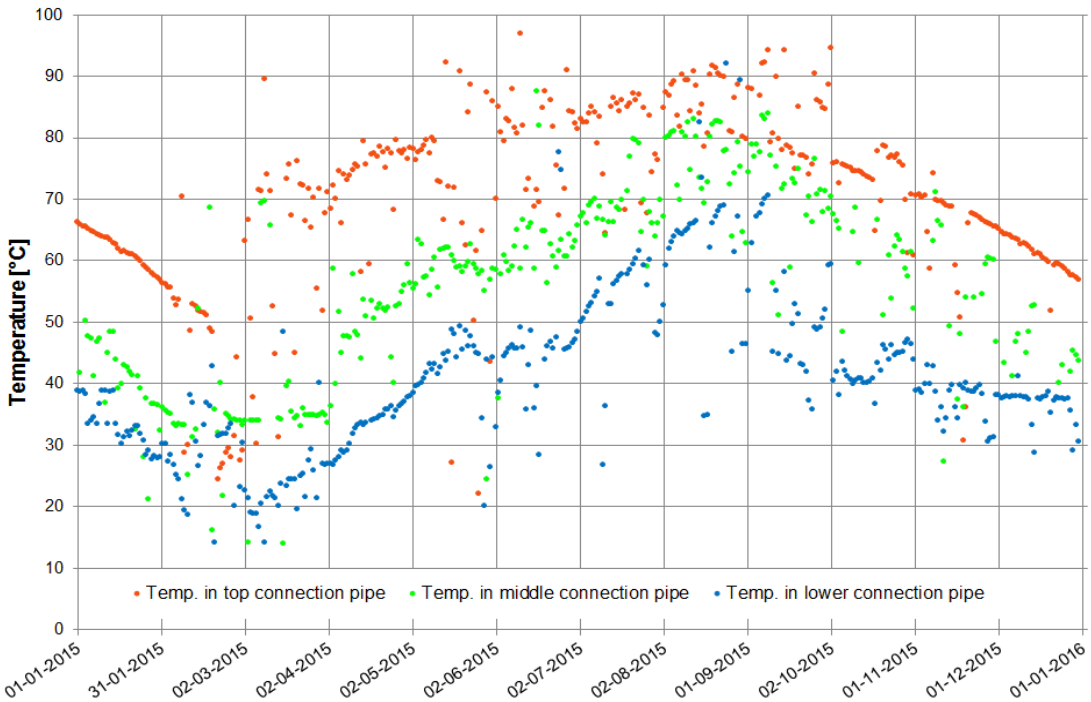

Fig. 31: Temperatures for PTES charging and discharging in 2015 (flow weighted daily mean values)

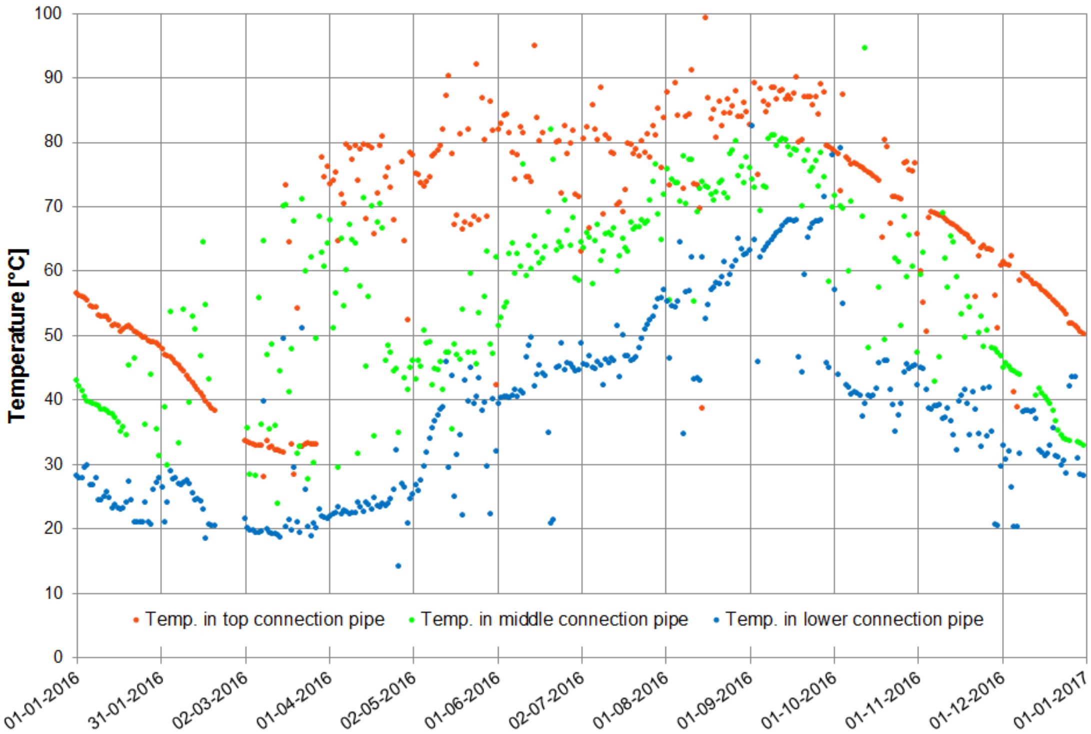

Fig. 32: Temperatures for PTES charging and discharging in 2016 (flow weighted daily mean values)

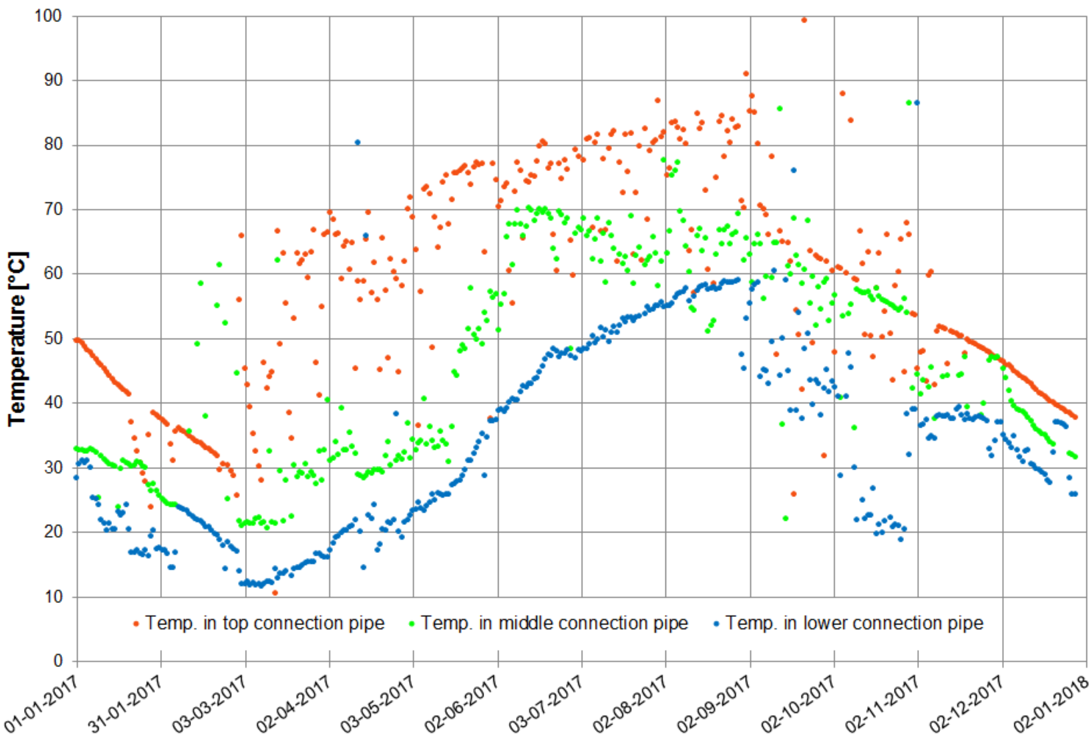

Fig. 33: Temperatures for PTES charging and discharging in 2017 (flow weighted daily mean values)

5.2. PTES ground temperatures

85 temperature sensors are installed inside and around the storage volume in order to allow an observation of the long-term temperature development in the storage volume and in the surrounding ground. Fig. 34 shows the locations where temperature sensors are placed in different horizontal and vertical positions.
The temperatures shown in Fig. 29 are from the storage internal position A1. The vertical positions inside the storage range from below the floating liner (0 m) down to the bottom liner at -16 m.
The sensors in the locations B to G are installed in the surrounding ground. C and B go down 2 m below the bottom of the PTES to a level of -18 m. The horizontal distance between B and C is 10 m.

A more detailed drawing of sensor positions and dimensions is given in Fig. 3.

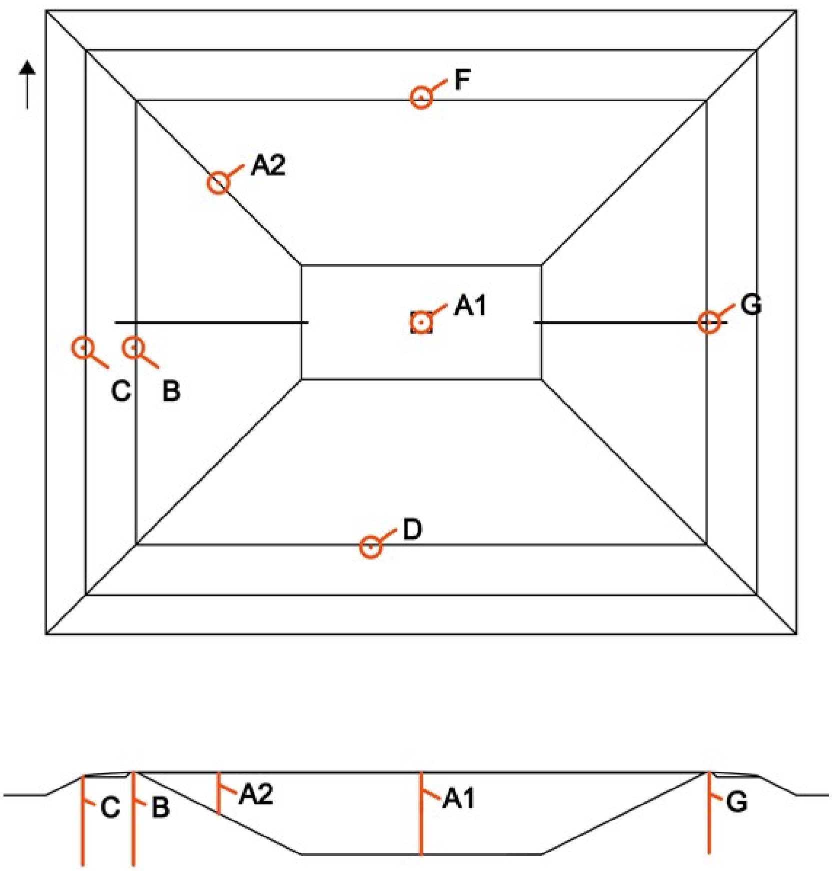

Fig. 34: Positions of temperature sensors inside and outside the PTES in Marstal (above: top view, below: side view).

Fig. 35 and Fig. 36 show ground temperatures at the positions B and C since 2013. The temperatures at the upper part of B and C show a seasonal variation with decreasing temperature levels and amplitudes with deeper locations and larger distances from the PTES side wall. The sensors approximately 10 m below the water surface show steady temperature increases that are heading towards their long-term limits at the end of the presented period.
Fig. 37 to Fig. 39 show the ground temperature developments at positions D, F and G. Considering the symmetry, the temperature developments show the same general tendencies with some deviations when comparing with corresponding sensor positions from the positions B.

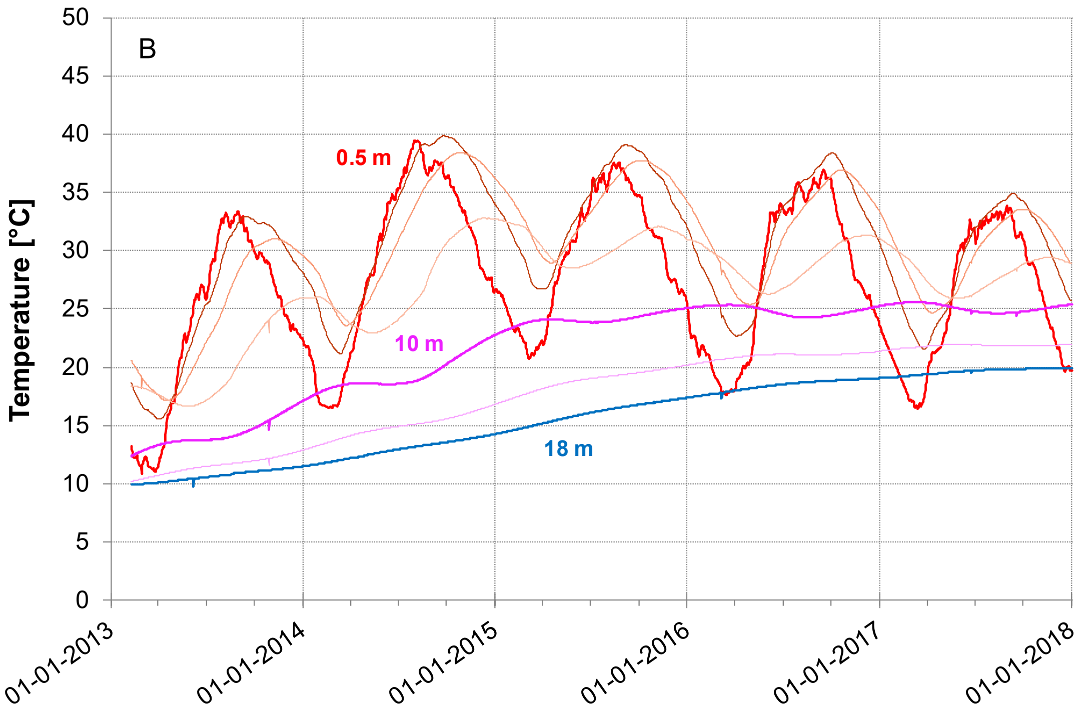

Fig. 35: Long-term ground temperature development at position "B" (see Fig. 34 or Fig. 3)

Fig. 40 and Fig. 41 show the monthly ground temperature development for 2017 in the east-west and the north-south axis in comparison to the temperatures inside the storage. In general, a symmetric temperature dispersion can be noted with a little higher ground temperatures in the east at position "G". At positions "B" at 12 m and "D" at 10 m layers with slight temperature increases can be observed.
For the years 2015 and 2016, the monthly ground temperature development can be found in Annex 2 in Fig. 51 to Fig. 54.

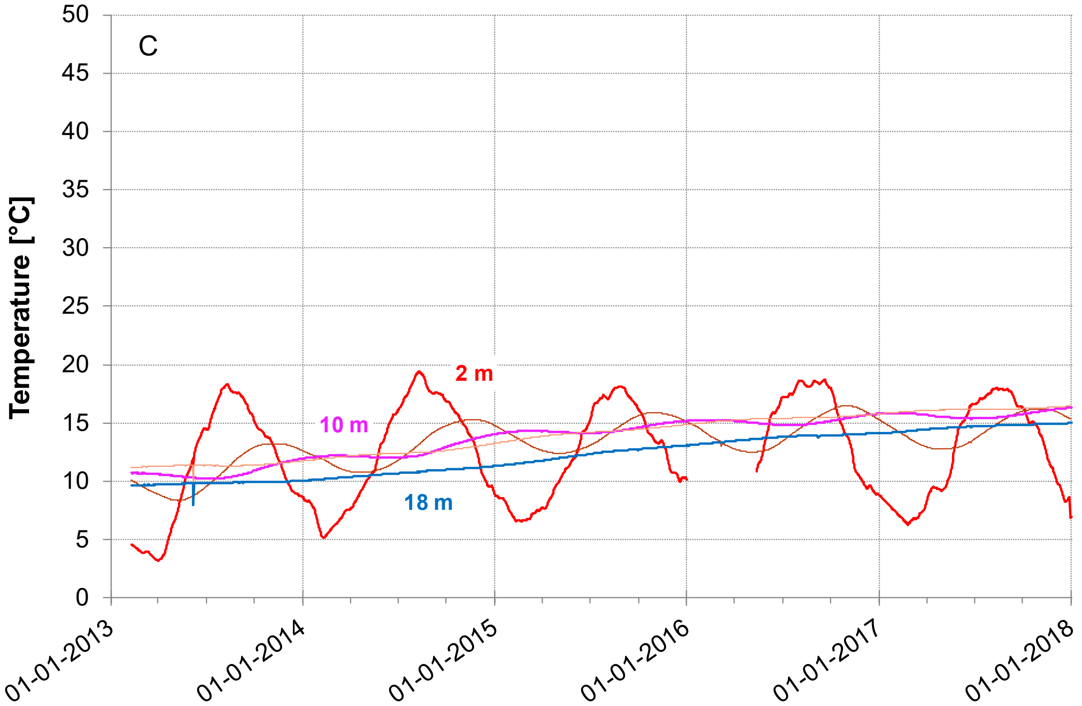

Fig. 36: Long-term ground temperature development at position “C” (see Fig. 34 or Fig. 3)

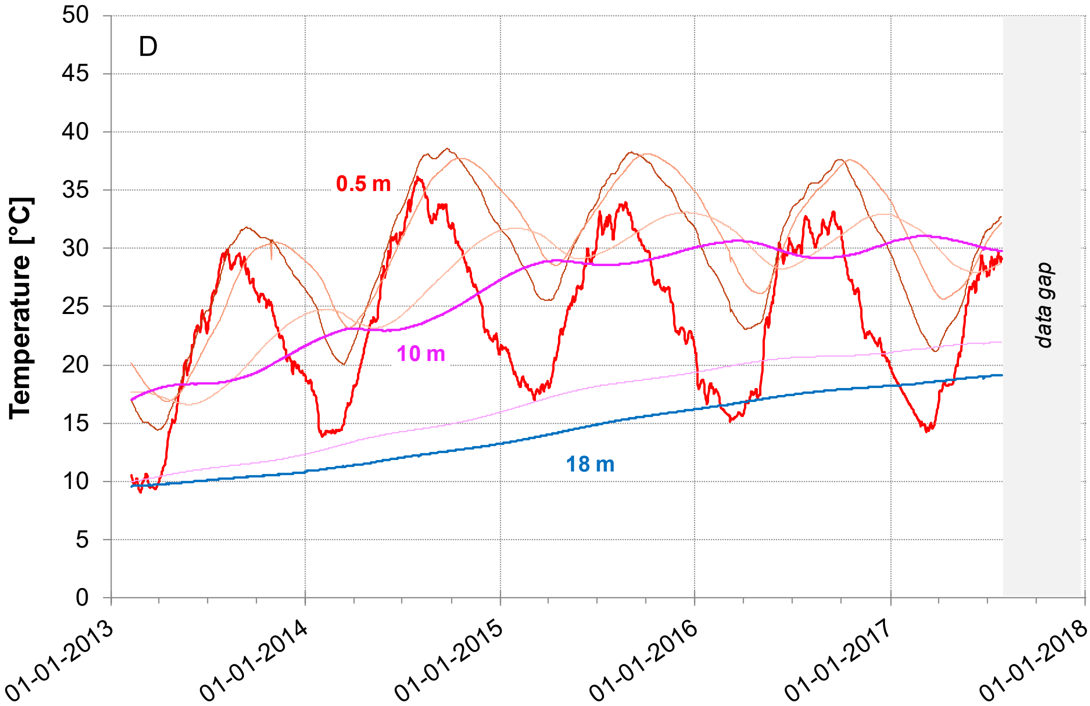

Fig. 37: Long-term ground temperature development at position “D” (see Fig. 34 or Fig. 3)

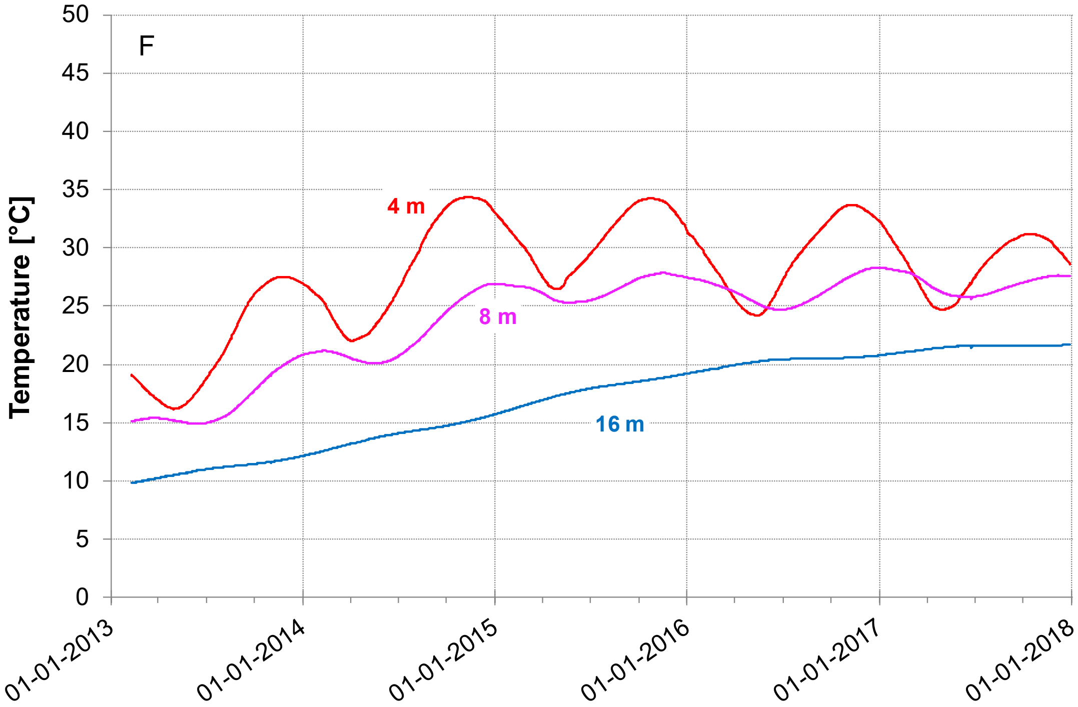

Fig. 38: Long-term ground temperature development at position “F” (see Fig. 34 or Fig. 3)

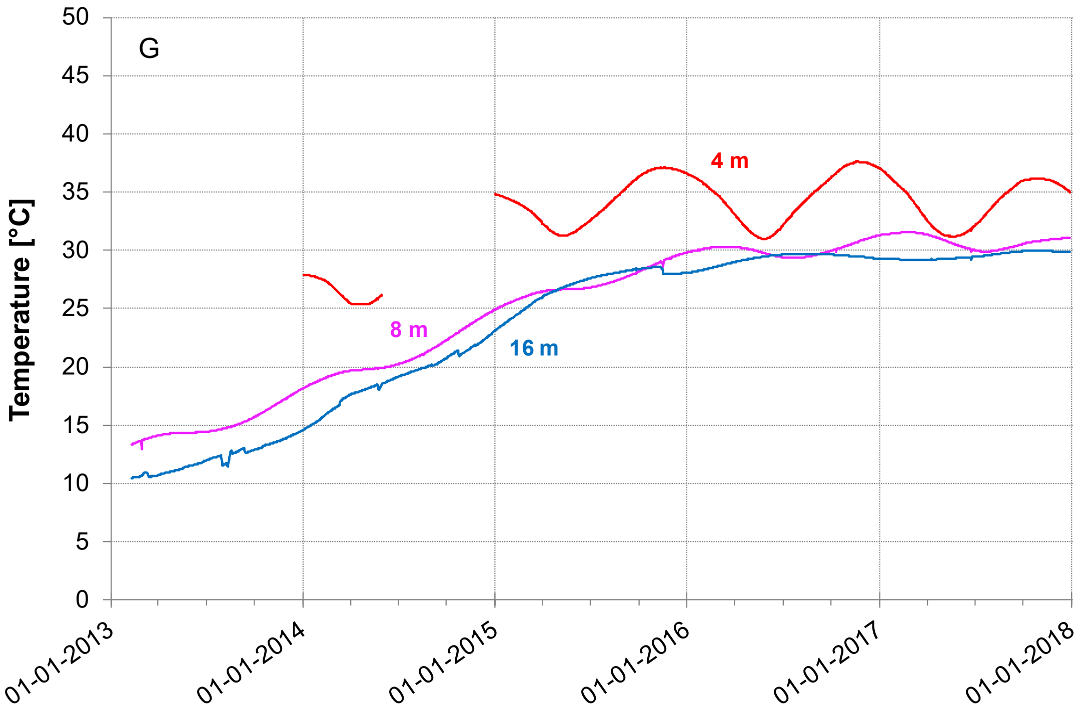

Fig. 39: Long-term ground temperature development at position “G” (see Fig. 34 or Fig. 3)

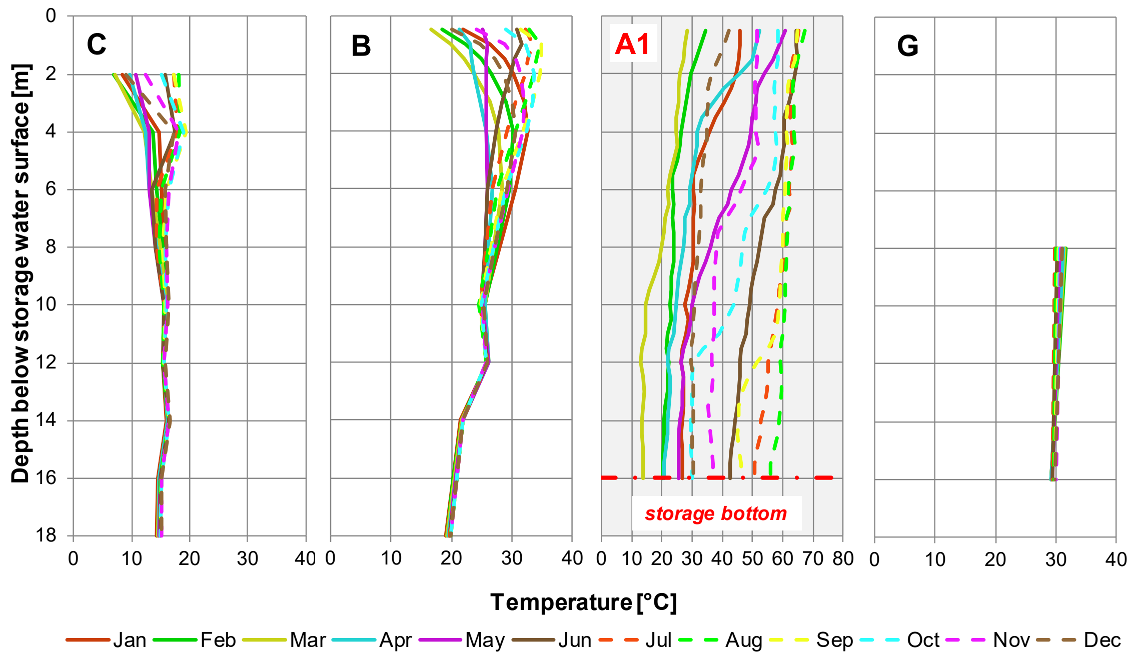

Fig. 40: Ground temperature development at positions “C”, “B” and “G” in comparison to “A1” in 2017 (see Fig. 34 or Fig. 3, daily mean values at mid of the months)

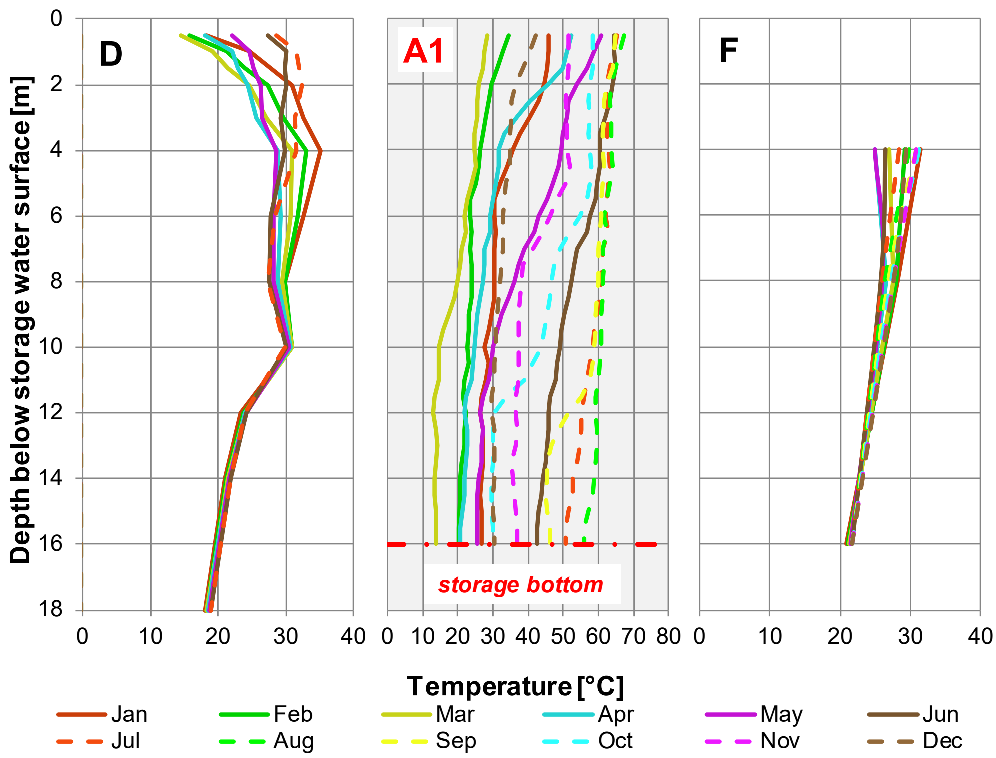

Fig. 41: Ground temperature development at positions “D” and “F” in comparison to “A1” in 2017 (see Fig. 34 or Fig. 3, daily mean values at mid of the months)

In the cover construction one heat flux sensor and a pair of temperature sensors were installed at the position A1 for observation of the cover heat losses. Fig. 42 and Fig. 43 show the development of the cover heat losses at this specific position in the years 2016 and 2017. The heat losses are depending on the temperature difference between the upper temperatures in the storage and the temperatures at the cover surface and vary between 20 and 65 W/m² cover area. The lowest heat losses occur in March, when the temperatures in the storage are the lowest. The highest heat losses can be seen end of summer.

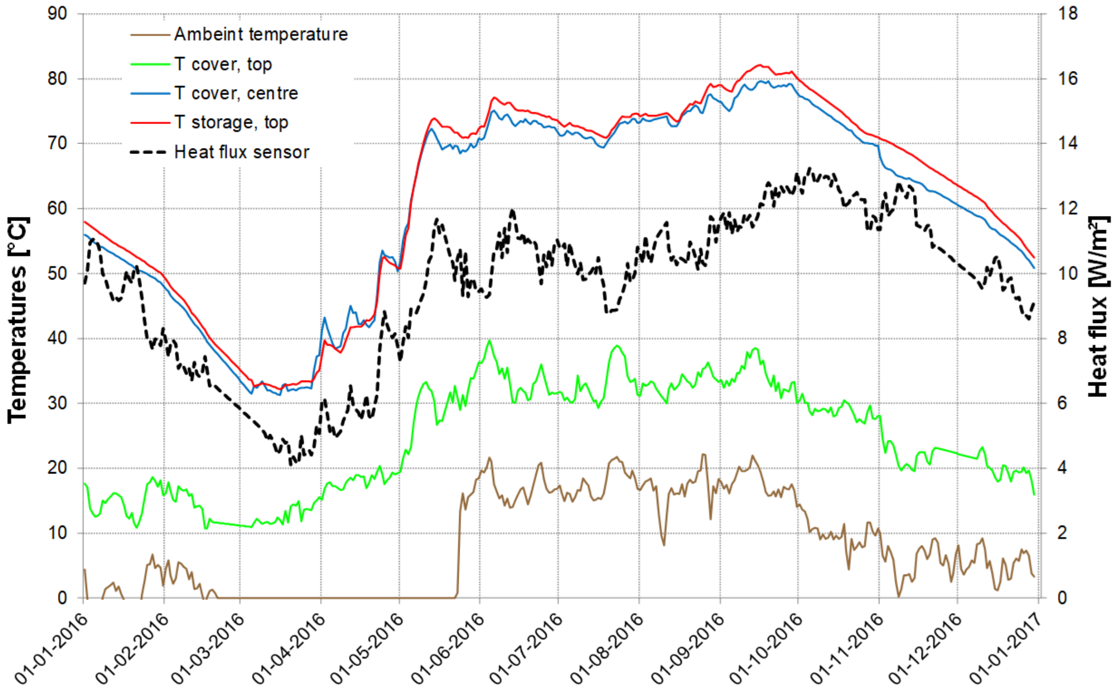

Fig. 42: development of temperatures and heat flux in the cover at position A1 (see Fig. 3) in 2016

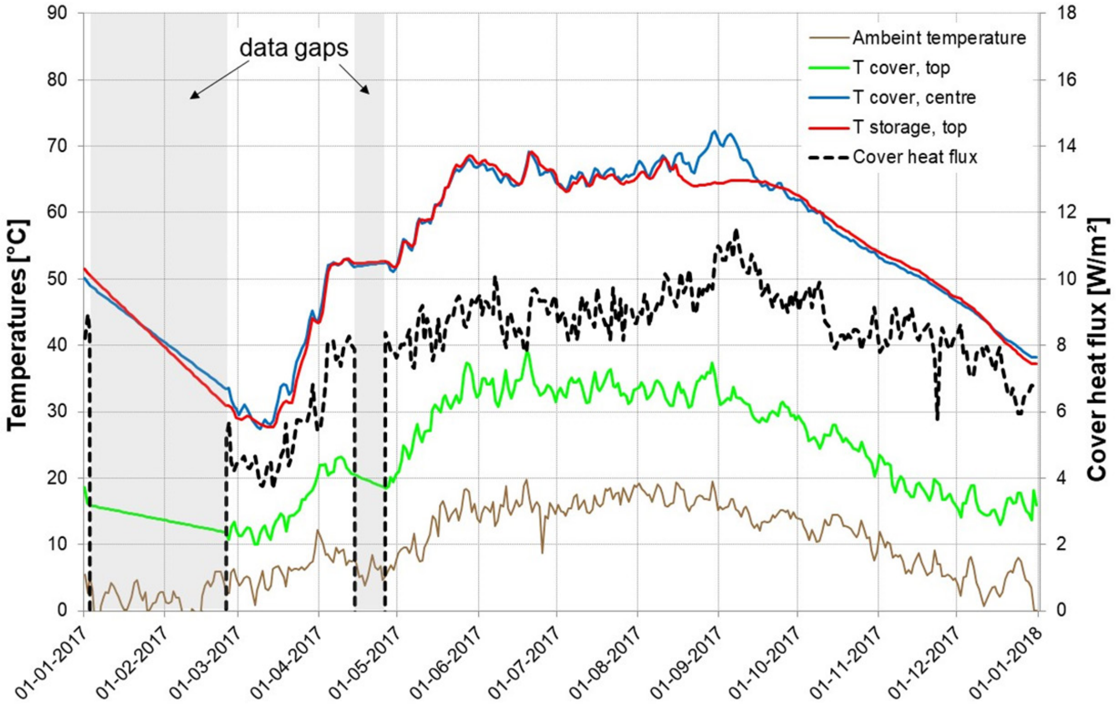

Fig. 43: development of temperatures and heat flux in the cover at position A1 (see Fig. 3) in 2017

6. HEAT PUMP

In Fig. 44 to Fig. 46 the monthly heat balances for the heat pump can be seen for 2015, 2016 and 2017. The main usage of the heat pump is in the heating season, preferably when electricity prices are low.
From the yearly heat production and electricity demand values yearly COP values of 3.3 can be calculated for 2015 and 2016 respectively, in 2017 the COP of 3.2 is slightly lower.

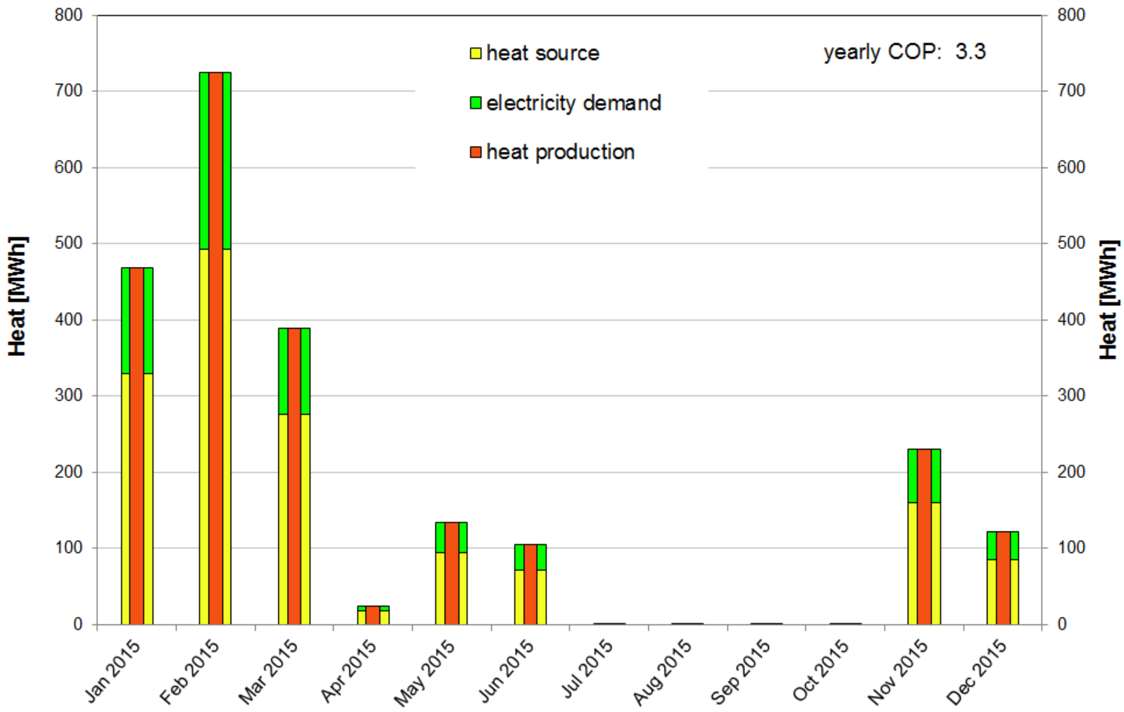

Fig. 44: Monthly heat balance of the heat pump in 2015

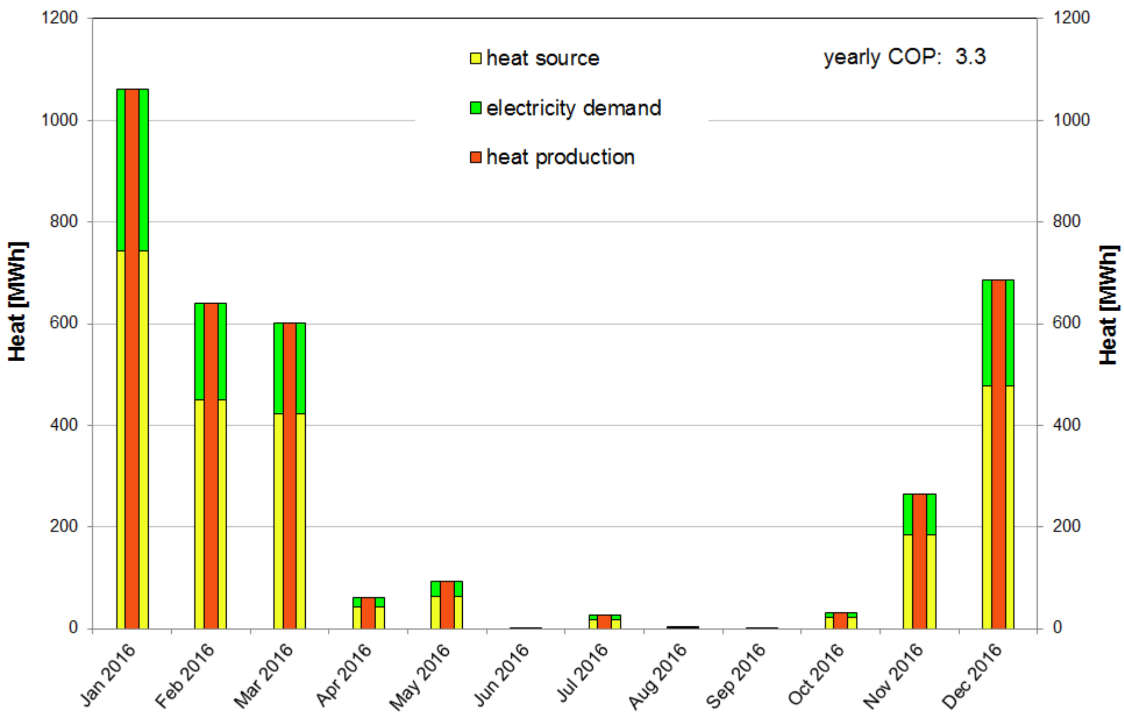

Fig. 45: Monthly heat balance of the heat pump in 2016

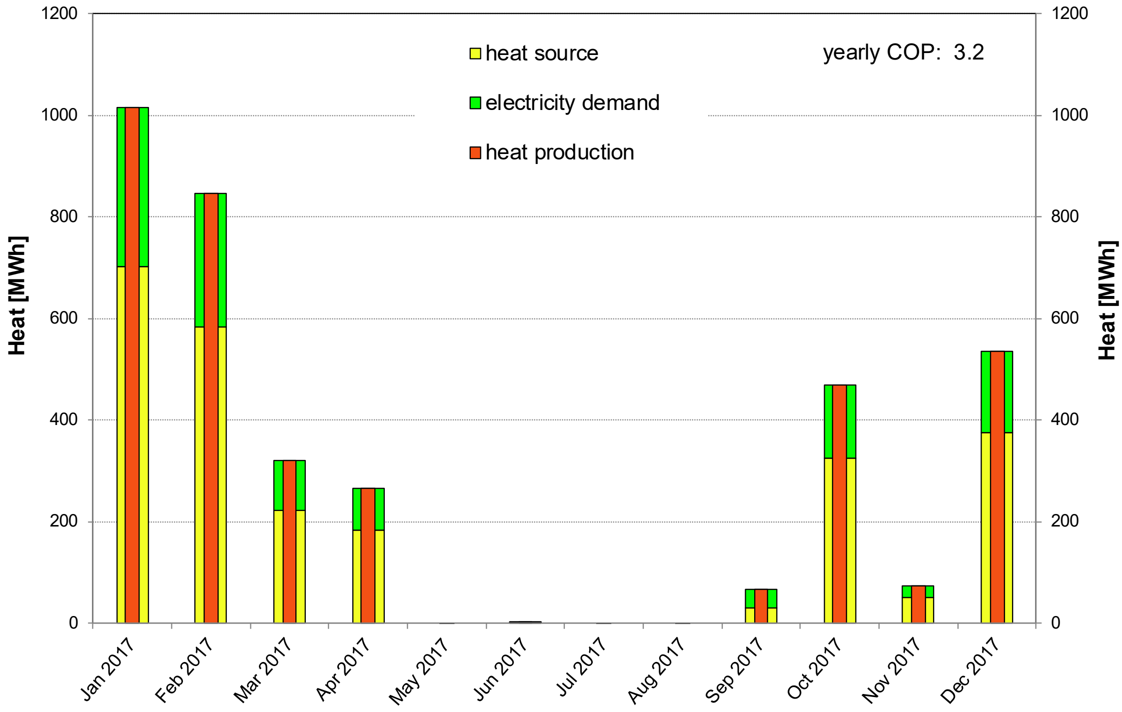

Fig. 46: Monthly heat balance of the heat pump in 2017

Fig. 47 to Fig. 49 show the rather similar operation conditions for the heat pump in the years 2015 to 2017. The condenser outlet temperatures are almost constant at 75 °C. Condenser inlet temperatures are below 40 °C. The evaporator inlet temperatures are depending on the PTES temperatures and vary between 60 and 30 °C in the operation period and the evaporator outlet temperatures are around 20 °C.

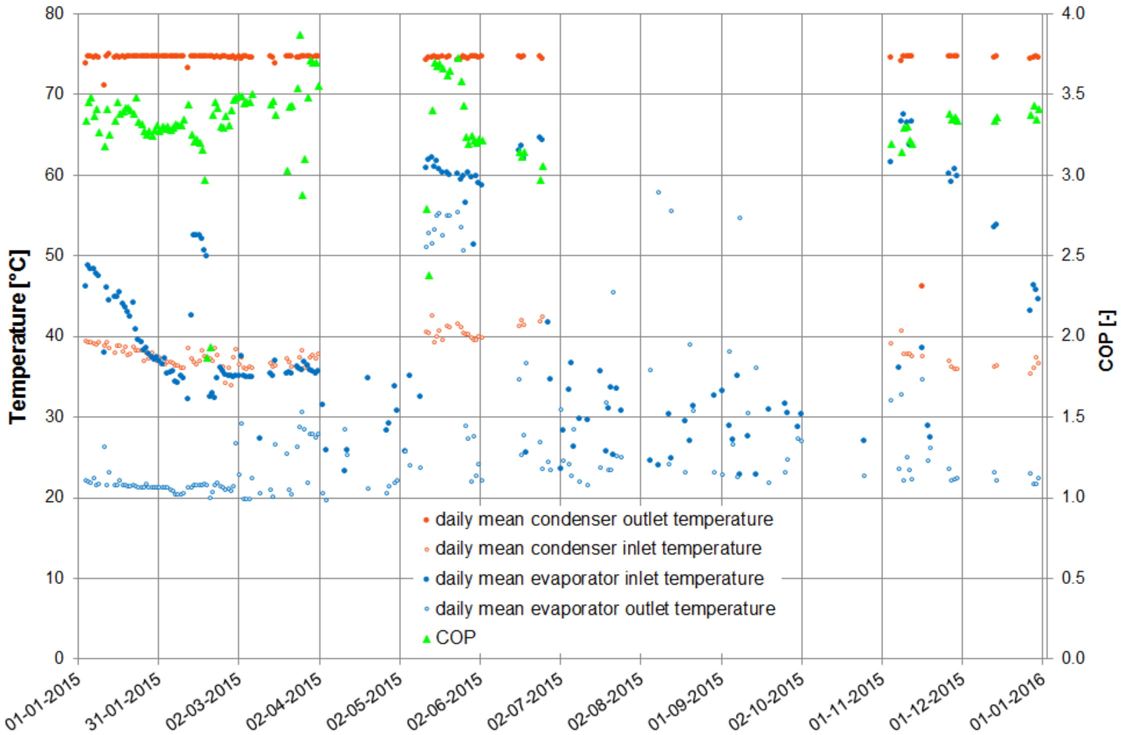

Fig. 47: Heat pump operation conditions in 2015 (weighted daily mean values)

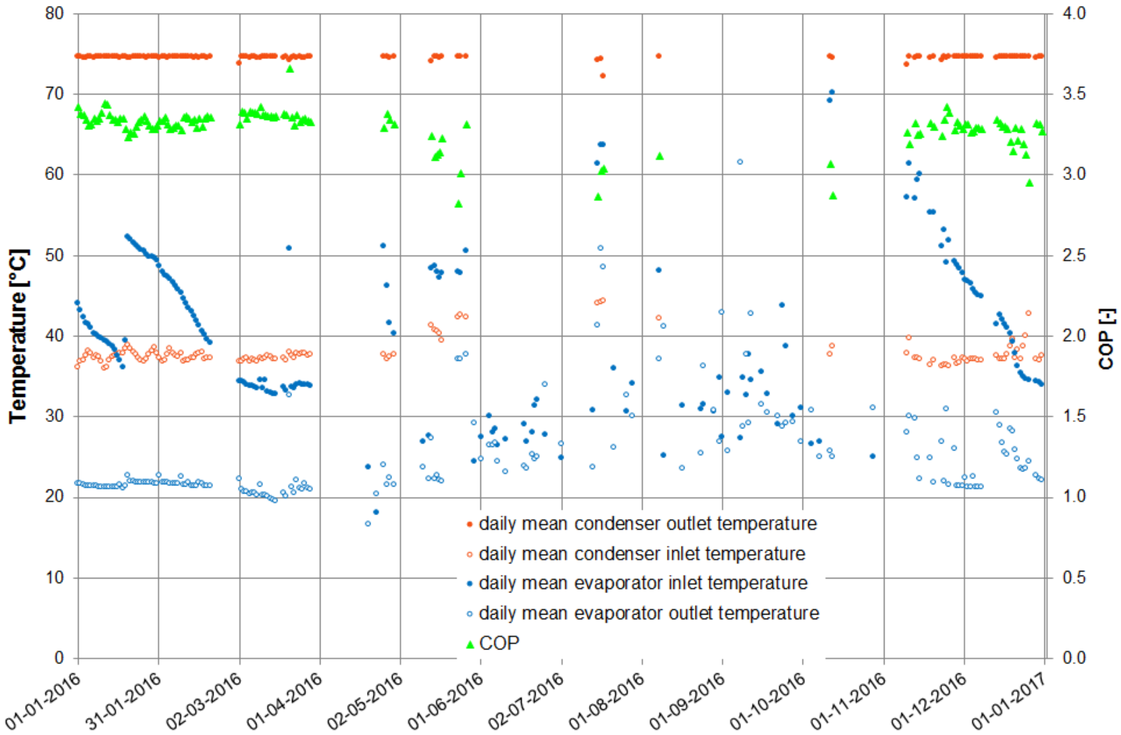

Fig. 48: Heat pump operation conditions in 2016 (weighted daily mean values)

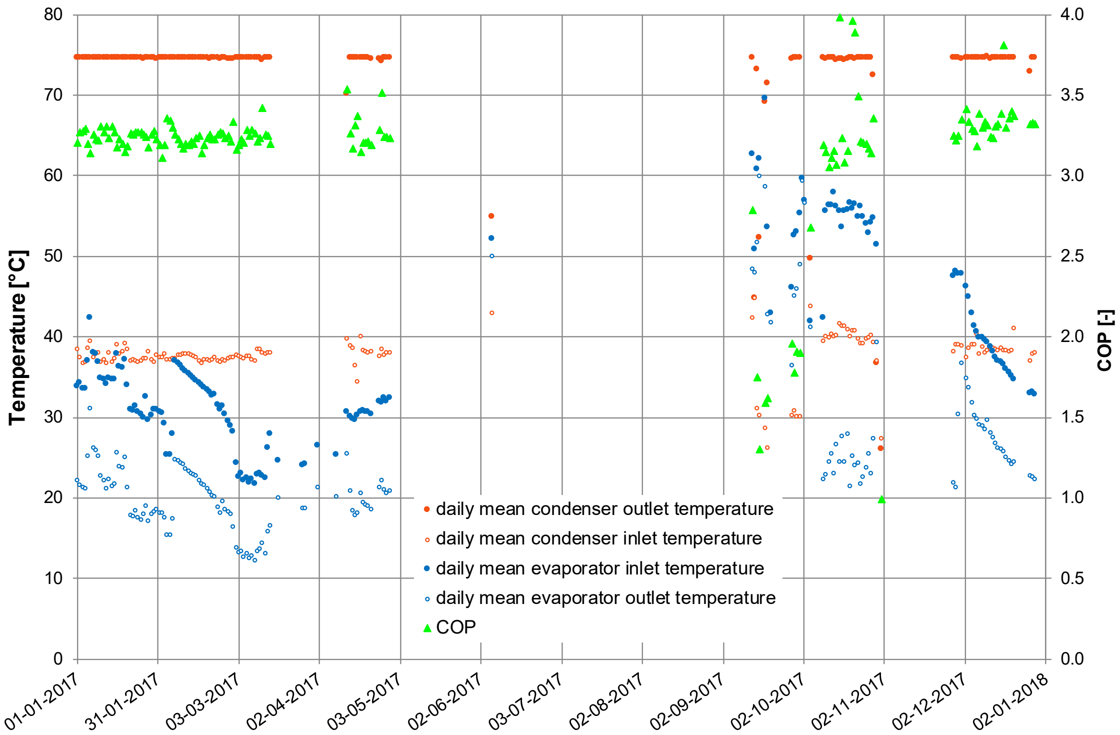

Fig. 49: Heat pump operation conditions in 2017 (weighted daily mean values)

7. SUMMARY

The evaluations for the years 2015 to 2017 for the SDH plant in Marstal confirm high solar fractions between 28 % and 39 %. In two of the three years, this value was higher than the design value of 32 %.

For the solar collector fields high solar yields of 320 to almost 450 kWh/m²a can be seen, depending on the solar collector product and the yearly solar irradiation.

The efficiency of the seasonal pit thermal energy storage was 66 % in 2015 and 2016. In 2017 a leakage in the top cover sheet of the storage caused most probably a humidification of a part of the cover insulation by rain water. The PTES data for 2017 shows lower temperatures in the summer period, less heat that was discharged from the storage during the year and much higher thermal losses compared to the years before. In the end a storage efficiency of only 39 % could be reached in 2017. The goal is to repair the leakage in short-term to allow for higher efficiencies again in the upcoming years.

With contributions of 54 to 59 %, the main heat source in Marstal is a biomass boiler that provides heat to an ORC unit and to the DH network. The backup oil boilers had only minor shares of 0, 8 and 13% in the past years. As the boilers are operated with bio-oil, the renewable share in Marstal was 100 % in the entire evaluation period.

When comparing the system energy balance with design values the results show good agreements with the predictions. This proves on the one hand side a high capability of the entire energy system and on the other hand a good quality of the design and prediction tools.

8. REFERENCES

Larsen et.al, 2014	Larsen L., Nielsen J., Battisti R., Hammerschmid, A., Malu M., Dalenbäck J.O., Février N., Depenau J., Sørensen P.A., Schmidt T., project final report to European FP7 project SUNSTORE 4, Grant agreement no. ENER/FP7/249800/"SUNSTORE 4
Schmidt, 2013	Schmidt, T., SUNSTORE 4 – Design of the measurement and evaluation programme, Deliverable 4.1 to European FP7 project SUNSTORE 4, Grant agreement no. ENER/FP7/249800/"SUNSTORE 4
Schmidt & Sørensen 2018	Schmidt, T., Sørensen, P.A.: Monitoring Results from Large Scale Heat storages for District Heating in Denmark, 14th International Conference on Energy Storage, 25-28 April 2018, Adana, Turkey
Schmidt et.al., 2014	Schmidt, T., Larsen L., Sørensen P.A., SUNSTORE 4 – Report on operation experiences and monitoring results after one year, Deliverable 4.2 to European FP7 project SUNSTORE 4, Grant agreement no. ENER/FP7/249800/"SUNSTORE 4
Schmidt et.al., 2014-2	Schmidt, T., Larsen L., Sørensen P.A., SUNSTORE 4 – Report on operation experiences and monitoring results after two years, Deliverable 4.3 to European FP7 project SUNSTORE 4, Grant agreement no. ENER/FP7/249800/"SUNSTORE 4
Sørensen, 2018:	Sørensen P.A., “Best practice” for implementation and operation of the Large Scale Borehole and Pit Heat Thermal Storages (BTES and PTES) in Brædstrup, Marstal, Dronninglund and Gram, Denmark, PlanEnergi 2018.
Sørensen et.al. 2018	Sørensen P.A., Larsen J., Larsen L., Frey J., Schmidt T., Bjørn H., Furbo S.: Follow up on large scale heat storages in Denmark, final report to EUDP project 64014-0121, PlanEnergi 2018

9. ANNEX 1: YEARLY HEAT BALANCE ACCORDING TO DESIGN CALCULATIONS

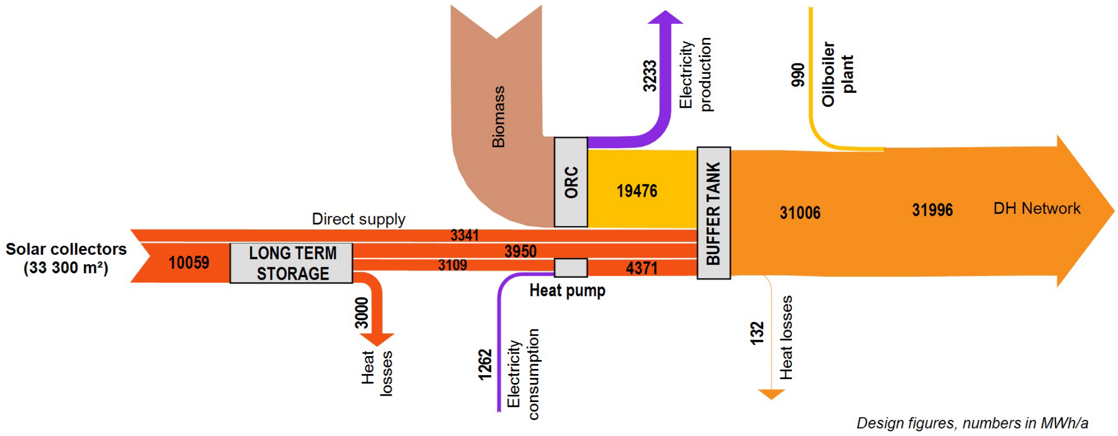

Fig. 50: Heat flow diagram according to design figures (source: PlanEnergi)

10. ANNEX 2: PTES GROUND TEMPERATURE DEVELOPMENT

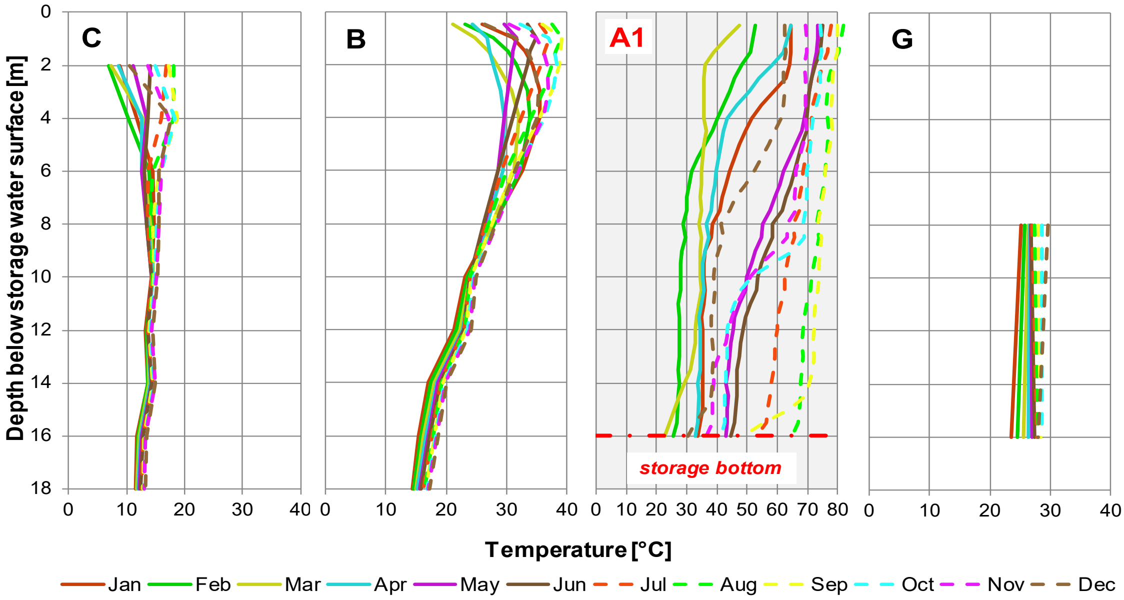

Fig. 51: Ground temperature development at positions “D” and “F” in comparison to “A1” in 2015 (see Fig. 34 or Fig. 3, daily mean values at mid of the months)

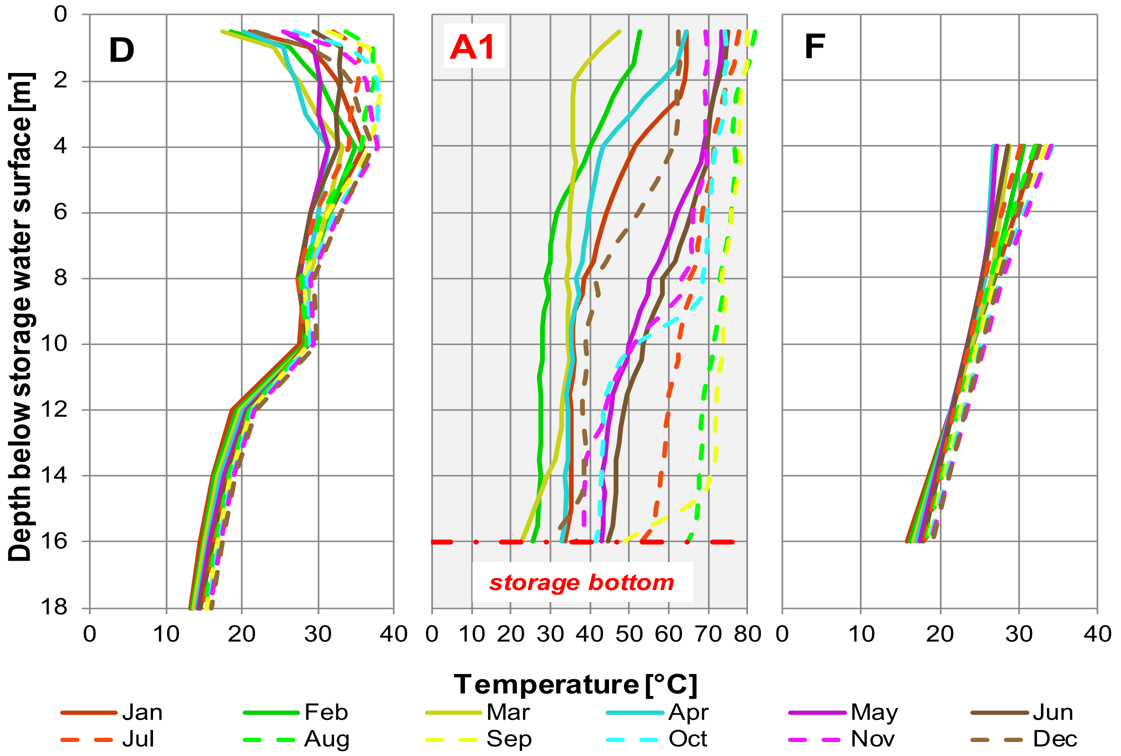

Fig. 52: Ground temperature development at positions “D” and “F” in comparison to “A1” in 2015 (see Fig. 34 or Fig. 3, daily mean values at mid of the months)

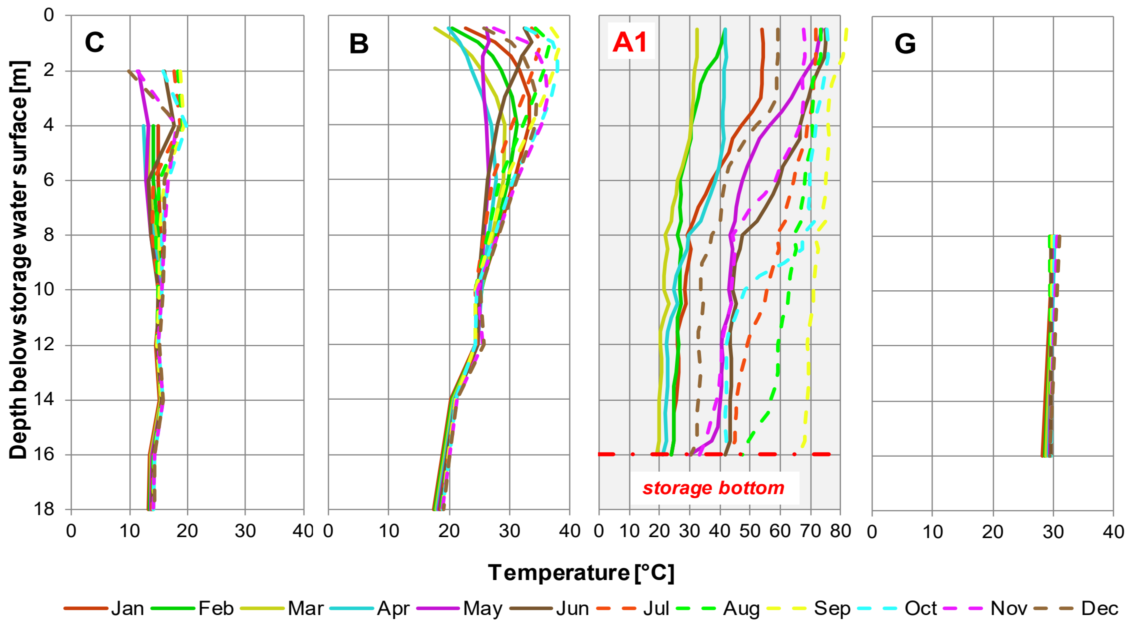

Fig. 53: Ground temperature development at positions “C”, “B” and “G” in comparison to “A1” in 2016 (see Fig. 34 or Fig. 3, daily mean values at mid of the months)

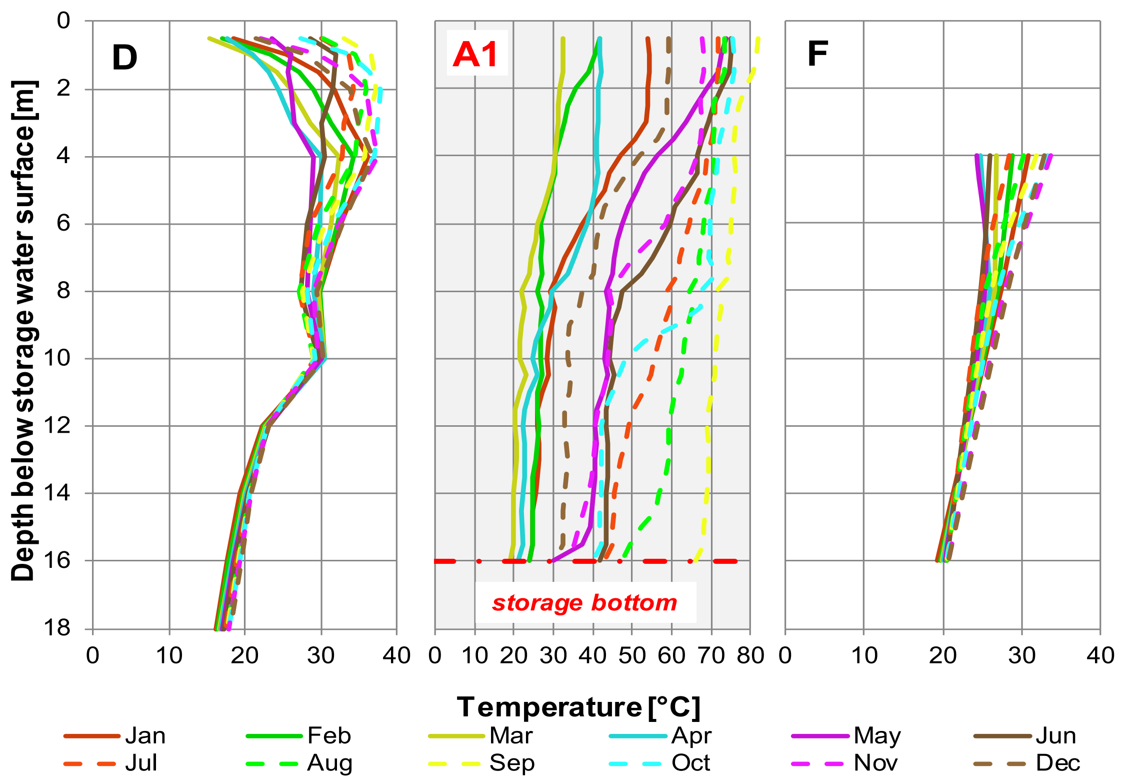

Fig. 54: Ground temperature development at positions “D” and “F” in comparison to “A1” in 2016 (see Fig. 34 or Fig. 3, daily mean values at mid of the months)